The lysosomal membrane protein SCAV-3 maintains lysosome integrity and adult longevity

Yuan Li,[1,2]* Baohui Chen,[2]* Wei Zou,[2]* Xin Wang,[3] Yanwei Wu,[2] Dongfeng Zhao,[2] Yanan Sun,[2] Yubing Liu,[2] Lianwan Chen,[4] Long Miao,[4] Chonglin Yang,[3] and Xiaochen Wang[2]

[1]College of Life Sciences, China Agriculture University, Beijing 100094, China
[2]National Institute of Biological Sciences, Beijing 102206, China
[3]State Key Laboratory of Molecular Developmental Biology, Institute of Genetics and Developmental Biology and [4]Institute of Biophysics, Chinese Academy of Sciences, Beijing 100101, China

Lysosomes degrade macromolecules and recycle metabolites as well as being involved in diverse processes that regulate cellular homeostasis. The lysosome is limited by a single phospholipid bilayer that forms a barrier to separate the potent luminal hydrolases from other cellular constituents, thus protecting the latter from unwanted degradation. The mechanisms that maintain lysosomal membrane integrity remain unknown. Here, we identified SCAV-3, the *Caenorhabditis elegans* homologue of human LIMP-2, as a key regulator of lysosome integrity, motility, and dynamics. Loss of *scav-3* caused rupture of lysosome membranes and significantly shortened lifespan. Both of these phenotypes were suppressed by reinforced expression of LMP-1 or LMP-2, the *C. elegans* LAMPs, indicating that longevity requires maintenance of lysosome integrity. Remarkably, reduction in insulin/insulin-like growth factor 1 (IGF-1) signaling suppressed lysosomal damage and extended the lifespan in *scav-3(lf)* animals in a DAF-16–dependent manner. Our data reveal that SCAV-3 is essential for preserving lysosomal membrane stability and that modulation of lysosome integrity by the insulin/IGF-1 signaling pathway affects longevity.

Introduction

Lysosomes degrade extra- and intracellular material delivered by endocytosis, phagocytosis, or autophagy and recycle catabolites for reutilization in cellular metabolism. There is increasing recognition that lysosomes are advanced organelles that perform much broader functions than cargo digestion and recycling and are involved in fundamental cellular processes such as plasma membrane repair, immune responses, nutrient sensing and signaling, and cell death. As a result, impairment of lysosome function contributes to the pathogenesis of many diseases including lysosomal storage diseases, neurodegenerative disorders, and cancer (Appelqvist et al., 2013; Settembre et al., 2013).

The lysosomal lumen contains ∽60 different soluble acid hydrolases that act in coordination to degrade all types of macromolecules (Settembre et al., 2013). With such a high enrichment of catabolic enzymes, lysosomes have long been considered "suicide bags." Lysosomal rupture causes leakage of the luminal contents into the cytosol, leading to membrane trafficking defects, abnormal energy metabolism, and cell death by means of apoptosis or necrosis (de Duve, 1983; Repnik et al., 2014). Thus, maintenance of lysosome integrity is clearly important for cell viability. On the other hand, induction or amplification of cell death events by lysosomal membrane permeabilization and the consequent release of lysosomal contents are considered alternative strategies for treating apoptosis- or multidrug-resistant cancers (Kreuzaler and Watson, 2012; Groth-Pedersen and Jäättelä, 2013; Kallunki et al., 2013).

As a safeguard, the lysosome is limited by a 7- to 10-nm single phospholipid bilayer, which serves as the mechanical barrier that encloses the potent luminal hydrolases and protects the other cellular constituents from unwanted degradation (Saftig et al., 2010). The lysosomal membrane contains heavily glycosylated membrane proteins, which may form a continuous carbohydrate layer at the luminal leaflet to prevent the membrane from being degraded by the lysosomal hydrolases (Fukuda, 1991). These major lysosomal glycoproteins include lysosomal-associated membrane protein (LAMP)-1, LAMP-2, lysosomal integral membrane protein (LIMP)-1/CD63, and LIMP-2. LAMP-1 and LAMP-2 have partially overlapping functions in vivo, but LAMP-2 seems to carry out additional unique functions such as acting as a receptor of chaperone-mediated autophagy (Eskelinen, 2006; Orenstein and Cuervo, 2010). LAMPs are thought to play an important protective role against lysosomal hydrolases owing to their very high

*Y. Li, B. Chen, and W. Zou contributed equally to this work.

Correspondence to Xiaochen Wang: wangxiaochen@nibs.ac.cn

Abbreviations used: ANOVA, analysis of variance; β-GCase, β-glucocerebrosidase; Gal, galectin; IGF-1, insulin-like growth factor 1; lf, loss-of-function; LG, linkage group; PNGase F, peptide *N*-glycosidase F; TEM, transmission electron microscopy; ts, temperature-sensitive.

The Rockefeller University Press $30.00
J. Cell Biol. Vol. 215 No. 2 167–185
https://doi.org/10.1083/jcb.201602090

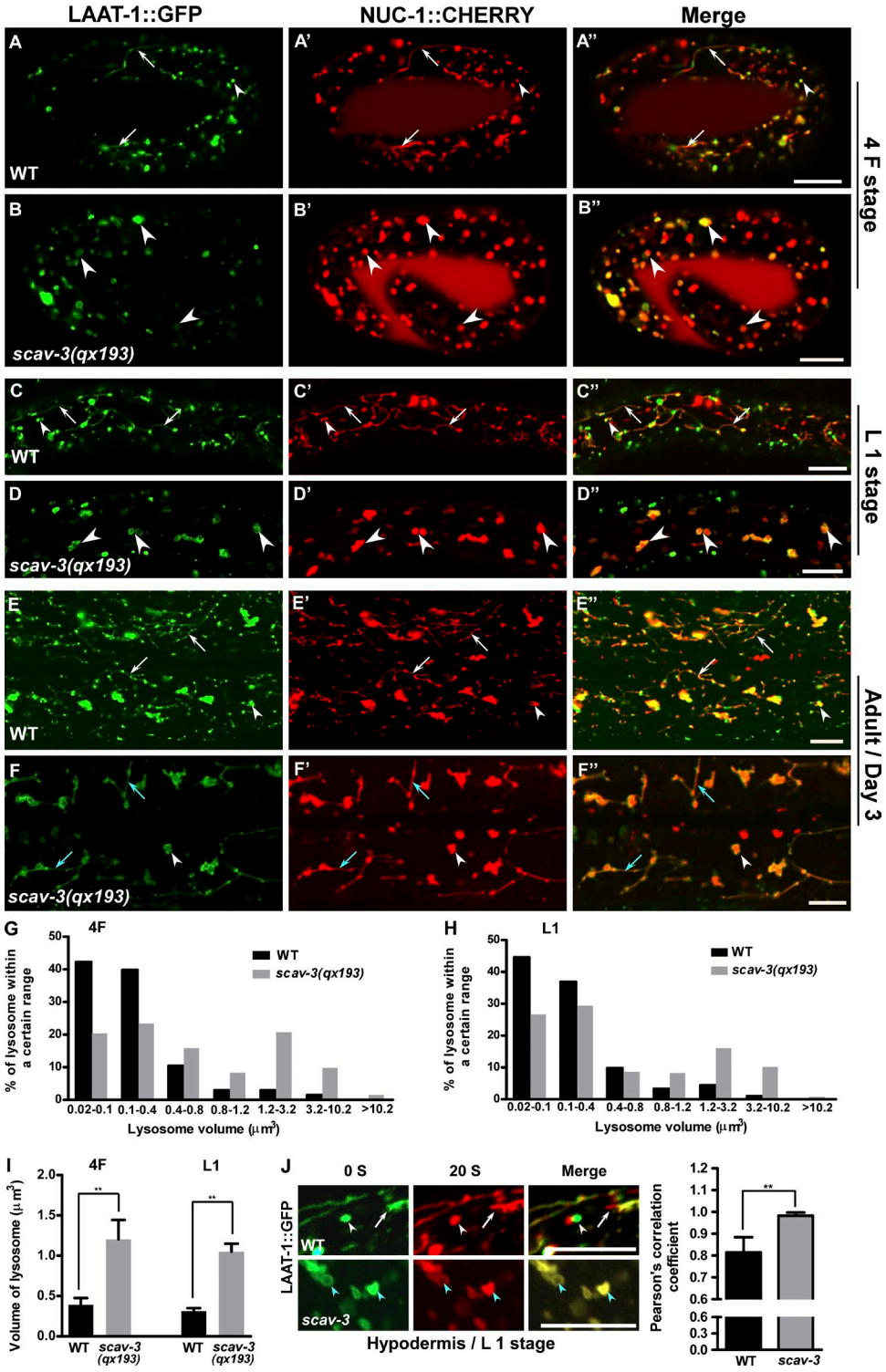

Figure 1. ***scav-3* mutants accumulate abnormal lysosomes.** (A–F″) Confocal fluorescent images of embryos (A–B″) and the hypodermis of larvae (C–D″) and adults (E–F″) in wild type (WT; A–A″, C–C″, and E–E″) and *scav-3(qx193)* (B–B″, D–D″, and F–F″) expressing LAAT-1::GFP and NUC-1::mCherry. Arrowheads, globular lysosomes; white arrows, tubular lysosomal structures; blue arrows, abnormal tubule-like structures in *scav-3(qx193)*. (G–I) Lysosome volumes in fourfold embryos (4F) or L1 larvae (L1) were quantified. At least 10 animals were scored in each strain at each stage. Data are shown as mean ± SD in I. Two-way ANOVA with the Bonferroni posttest was performed to compare mutant datasets with wild type. **, P < 0.001. (J) Time-lapse images of lysosomes in the hypodermis of L1 larvae of wild type and *scav-3(qx193)* expressing LAAT-1::GFP, with time point 0 s in green and 20 s in red. The overlay (merge) shows lysosome movement over time. White arrowheads and arrows, dynamic changes in globular and tubular lysosomes in wild type; blue arrowheads, static vesicular lysosomes in *scav-3(qx193)*. Pearson's correlation coefficient was determined and is shown in the right panel. Data are shown as mean ± SD. At least 10 movies were analyzed in each strain. Data were compared with the unpaired *t* test. **, P < 0.0001. Bars, 10 µm.

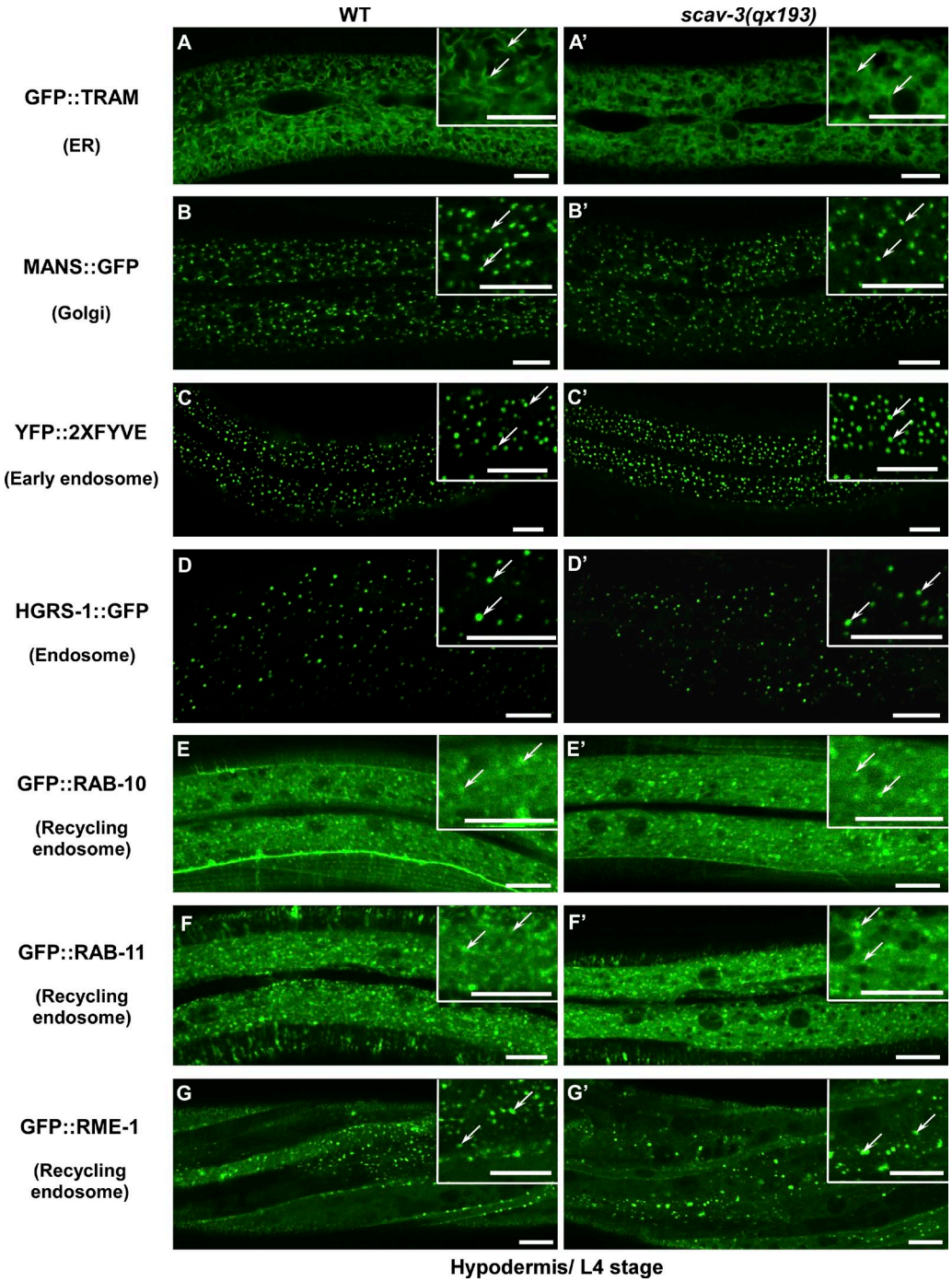

Figure 2. ***scav-3(qx193)* mutants contain normal endosomes, ER, and Golgi.** Confocal fluorescent images of the hypodermis in wild-type (WT) and *scav-3(qx193)* larvae expressing GFP::TRAM (A and A′), MANS::GFP (B and B′), YFP::2xFYVE (C and C′), HGRS-1::GFP (D and D′), GFP::RAB-10 (E and E′), GFP::RAB-11 (F and F′), or GFP::RME-1 (G and G′). Insets shows magnified views. Arrows indicate typical labeled structures. Bars, 10 µm.

abundance and the extensive glycosylation of their large intraluminal domain. However, in LAMP-1/LAMP-2 double-deficient MEF cells, lysosomal integrity is not affected (Eskelinen et al., 2004). In oncogene-transformed embryonic fibroblasts, decreased LAMP levels contribute to the sensitization of the cells to lysosomal cell death induced by various anticancer drugs. The cell death process is characterized by lysosomal membrane permeabilization and the subsequent release of cathepsins into the cytosol, suggesting a role of LAMPs in promoting lysosomal membrane stability in transformed cells (Fehrenbacher et al., 2008). Nevertheless, depletion of *lamp1* and *lamp2* has no effect on the sensitivity of nontransformed fibroblasts to agents that trigger lysosomal leakage (Fehrenbacher et al., 2008). Moreover, deglycosylation of LAMP-1 and LAMP-2 by endoglycosidase H, which removes Asn-linked glycans, causes rapid degradation of LAMPs but has no measurable effect on lysosomal pH, osmotic stability, density, or cell survival (Kundra and Kornfeld, 1999). Thus, the function of LAMPs in maintaining lysosomal membrane integrity under physiological conditions remains elusive.

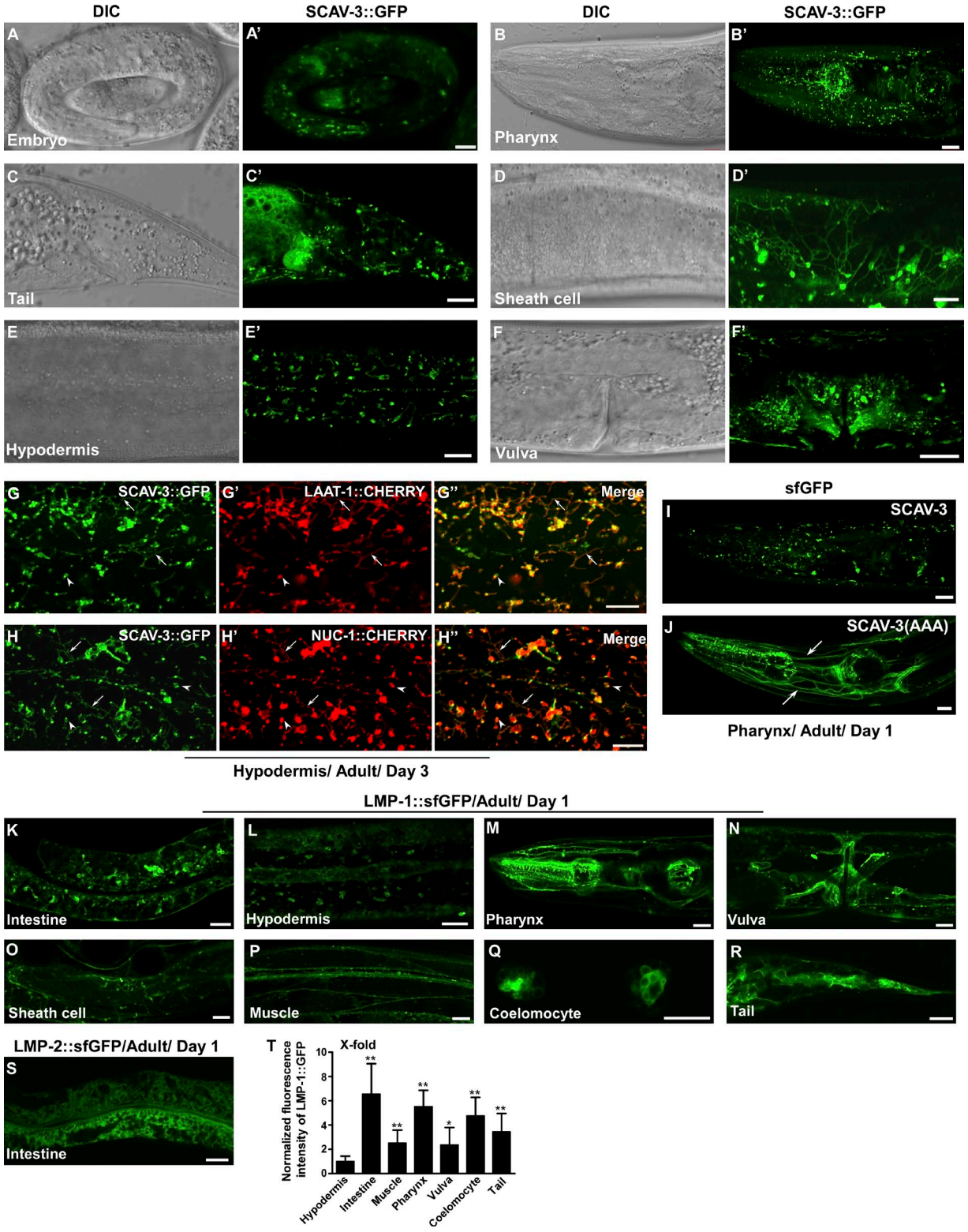

Figure 3. **SCAV-3 is widely distributed and localizes to lysosomes.** (A–F′) Differential interference contrast (DIC) and confocal fluorescent images of wild type expressing SCAV-3::GFP driven by the *scav-3* promoter. (G–H″) Confocal fluorescent images of the hypodermis in wild type expressing SCAV-3::GFP and LAAT-1::mCherry (G–G″) or SCAV-3::GFP and NUC-1::mCherry (H–H″). SCAV-3 colocalizes with LAAT-1 and NUC-1 to both vesicular (arrowheads) and tubular (arrows) lysosomes. (I and J) Fluorescent images of wild-type animals expressing SCAV-3::sfGFP (I) or SCAV-3(AAA)::sfGFP (J) in the pharynx. SCAV-3(AAA)::sfGFP localizes to plasma membranes (arrows). (K–S) Confocal fluorescent images of wild type expressing LMP-1::sfGFP (K–R) or LMP-2::sfGFP (S). (T) The mean total fluorescence intensity of LMP-1::sfGFP in different cell types was measured, and the normalized florescence intensity is shown. At least 15 animals were scored in each cell type. Data are shown as mean ± SD. One-way ANOVA with Tukey's posttest was performed to compare all the other datasets with hypodermis. *, $P < 0.05$; **, $P < 0.0001$. Bars, 10 µm.

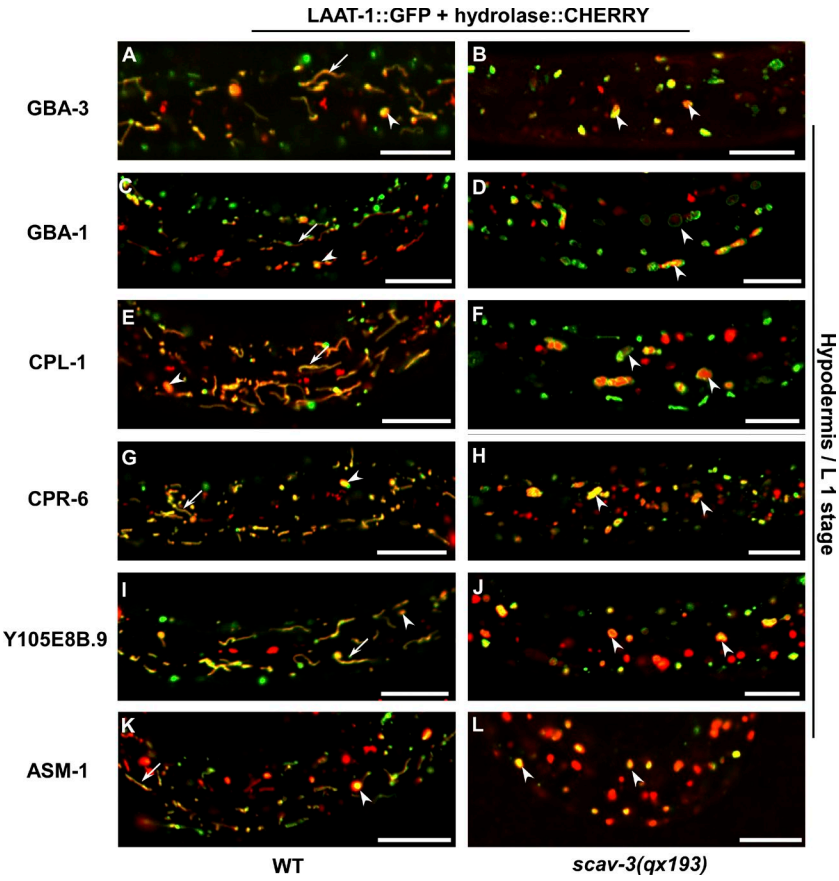

Figure 4. **Loss of *scav-3* does not affect targeting of lysosomal hydrolases.** Merged confocal fluorescent images of the hypodermis in wild-type (WT; A, C, E, G, I, and K) and *scav-3(qx193)* (B, D, F, H, J, and L) larvae coexpressing LAAT-1::GFP and GBA-3::mCherry (A and B), GBA-1::mCherry (C and D), CPL-1::mCherry (E and F), CPR-6::mCherry (G and H), Y105E8B.9::mCherry (I and J), or ASM-1::mCherry (K and L). The hydrolases were seen in LAAT-1::GFP-positive globular (arrowheads) and tubular (arrows) lysosomes in wild type and enlarged vesicular lysosomes (arrowheads) in *scav-3(qx193)* mutants. Bars, 10 µm.

It is worth noting that endoglycosidase H treatment, which was performed in living cells with special genetic and pharmacologic manipulations to prevent formation of complex oligosaccharide chains that are insensitive to this enzyme, does not affect the stability of LIMP-2, another major glycoprotein on the lysosomal membrane, implying that LIMP-2 may be involved in preserving the integrity of lysosomes (Kundra and Kornfeld, 1999). LIMP-2 is a ubiquitously expressed type III transmembrane protein that spans the membrane twice, with both N and C termini exposed to the cytosol and a large luminal domain containing complex carbohydrate structures (Vega et al., 1991). LIMP-2 has been identified as a receptor that mediates the mannose 6-phosphate–independent lysosomal targeting of β-glucocerebrosidase (β-GCase), the enzyme defective in Gaucher disease (Reczek et al., 2007). In this process, the luminal domain of LIMP-2 binds to β-GCase in the ER at neutral pH; the two proteins disassociate upon arrival at the lysosome because of the low pH (Blanz et al., 2010; Zachos et al., 2012 Neculai et al., 2013). In addition to mediating β-GCase transport, LIMP-2 was found to serve as a receptor for several enteroviruses that associate with hand, foot, and mouth disease and neurological diseases (Gonzalez et al., 2014). Moreover, overexpression of LIMP-2 in mammalian cells causes enlarged vacuoles that share both endosomal and lysosomal features, suggesting that LIMP-2 may be involved in the biogenesis of lysosomes/endosomes (Kuronita et al., 2002). Consistent with this, LIMP-2–deficient mice display phenotypes that may be caused by impaired membrane trafficking (Gamp et al., 2003; Saftig et al., 2010). However, it is unclear whether LIMP-2 plays a role in maintaining the integrity of lysosomes.

Lysosomes are the final degradative compartment downstream of various proteolytic pathways. Lysosome functions appear to decline during aging, which may account at least in part for the reduced protein degradation in older organisms and may contribute to various age-related pathologies (Hochschild, 1971; Cuervo and Dice, 2000). Consistent with this, age-related changes in lysosomes, such as increased volume, accumulation of indigestible materials, and fragility, are observed in senescent organisms (Hochschild, 1971; Terman and Brunk, 1998; Cuervo and Dice, 2000). It is unknown, however, whether lysosome activities are modulated during aging by longevity-regulating pathways. One such pathway is the insulin/insulin-like growth factor 1 (IGF-1) signaling cascade, which controls aging in *Caenorhabditis elegans*, insects, and mammals and extends the lifespan of these organisms when attenuated (Anisimov and Bartke, 2013). In worms, reduced insulin/IGF-1 signaling, such as that caused by mutation in the *daf-2* gene, which encodes the sole *C. elegans* insulin/IGF-1 receptor, leads to significantly increased adult longevity. This process involves a phosphorylation cascade that ultimately results in nuclear translocation of the DAF-16/FOXO transcription factor and subsequent transcriptional regulation of its target genes (Murphy and Hu, 2013).

In this study, we identify SCAV-3, the *C. elegans* homologue of human LIMP-2, as a key regulator of lysosome integrity and dynamics. Loss of *scav-3* causes lysosomal damage and shortened lifespan, which can be efficiently suppressed by inhibiting insulin/IGF-1 signaling in a DAF-16–dependent manner. Thus, lysosome integrity is modulated by the insulin/IGF-1 signaling pathway and is crucial for longevity.

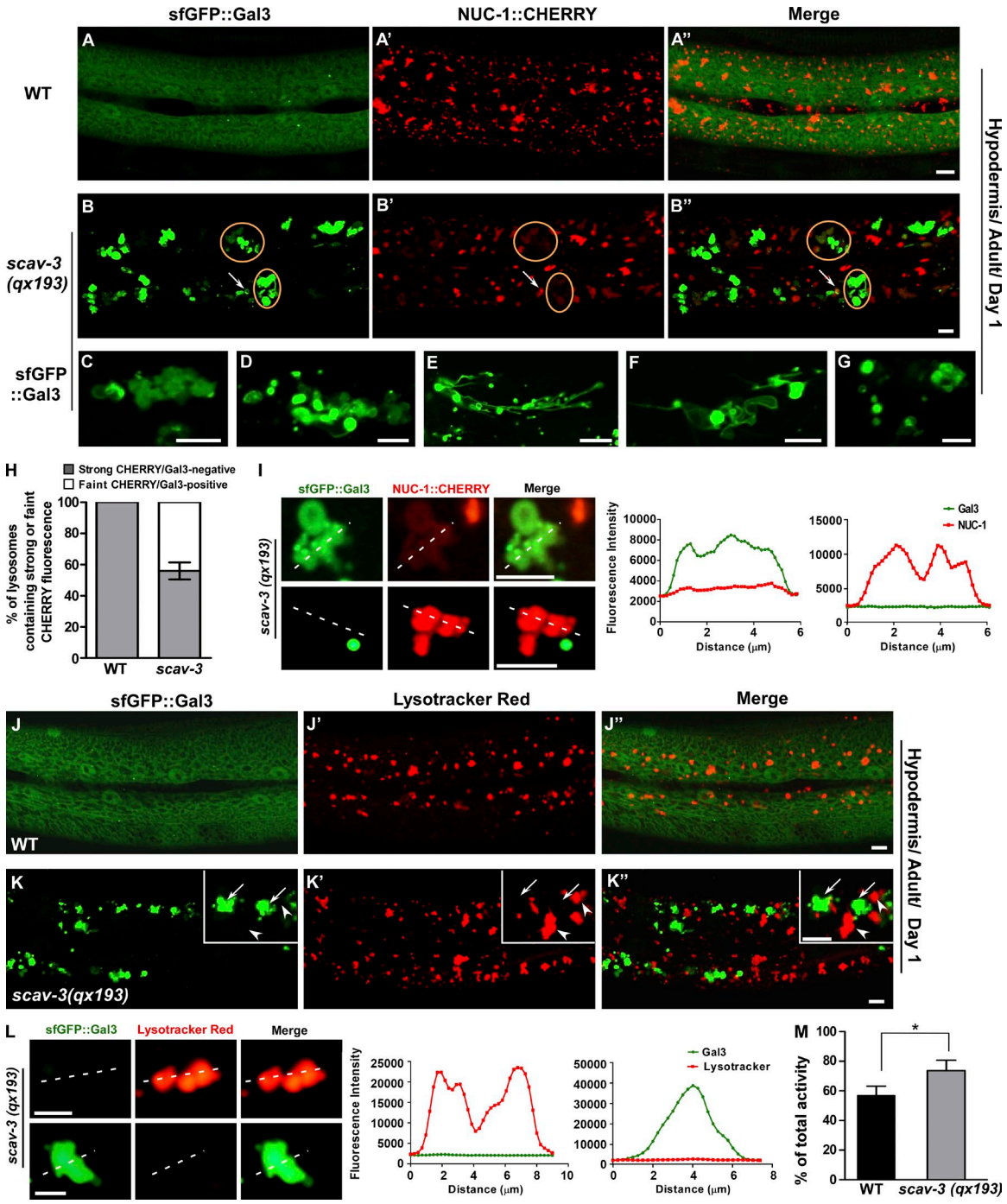

Figure 5. ***scav-3* mutants accumulate damaged lysosomes.** (A–G) Confocal fluorescent images of the hypodermis in wild-type (WT; A–A″) and *scav-3(qx193)* (B–B″ and C–G) adults expressing NUC-1::mCherry and/or sfGFP::Gal3. sfGFP::Gal3-positive structures contain faint NUC-1::mCherry fluorescence (B–B″, circles). A ring of sfGFP::Gal3 surrounding a bright NUC-1::mCherry punctum in *scav-3(qx193)* is indicated by the arrows. (H) The percentage of lysosomes that contain strong mCherry fluorescence and are negative for GFP::Gal3 (intact) and those that contain faint mCherry fluorescence and are positive for GFP::Gal3 (damaged) was quantified in wild type and *scav-3(qx193)* expressing sfGFP::Gal3 and NUC-1::mCherry. At least 15 animals were scored in each strain, and data are shown as mean ± SD. (I) Confocal fluorescent images and linescan analysis of lysosomes in *scav-3(qx193)* adults expressing sfGFP::Gal3 and NUC-1::mCherry. sfGFP::Gal3-positive structures contain faint NUC-1::mCherry fluorescence, whereas lysosomes with bright NUC-1::mCherry lacked sfGFP::Gal3. At least 10 lysosomes were examined, and the representative result is shown. (J–K″) Confocal fluorescent images of the hypodermis in wild-type (J–J″) and *scav-3(qx193)* (K–K″) adults expressing sfGFP::Gal3 and stained by LysoTracker red. Arrows and arrowheads indicate sfGFP::Gal3-positive and LysoTracker red–positive structures, respectively. (L) Confocal fluorescent images and linescan analysis of lysosomes in *scav-3(qx193)* adults expressing sfGFP::Gal3 and stained by LysoTracker red. sfGFP::Gal3-positive structures were not stained by LysoTracker red, whereas sfGFP::Gal3 was absent from LysoTracker red–positive vesicles. At least 10 lysosomes were examined, and the representative result is shown. (M) The available acid phosphatase activity in suspensions of wild-type and *scav-3(qx193)* lysosomes was determined, and the mean percentage of total activity (obtained in the presence of 0.1% Triton X-100) is shown. Data were compared with the unpaired *t* test. *, $P < 0.05$. Bars, 5 µm.

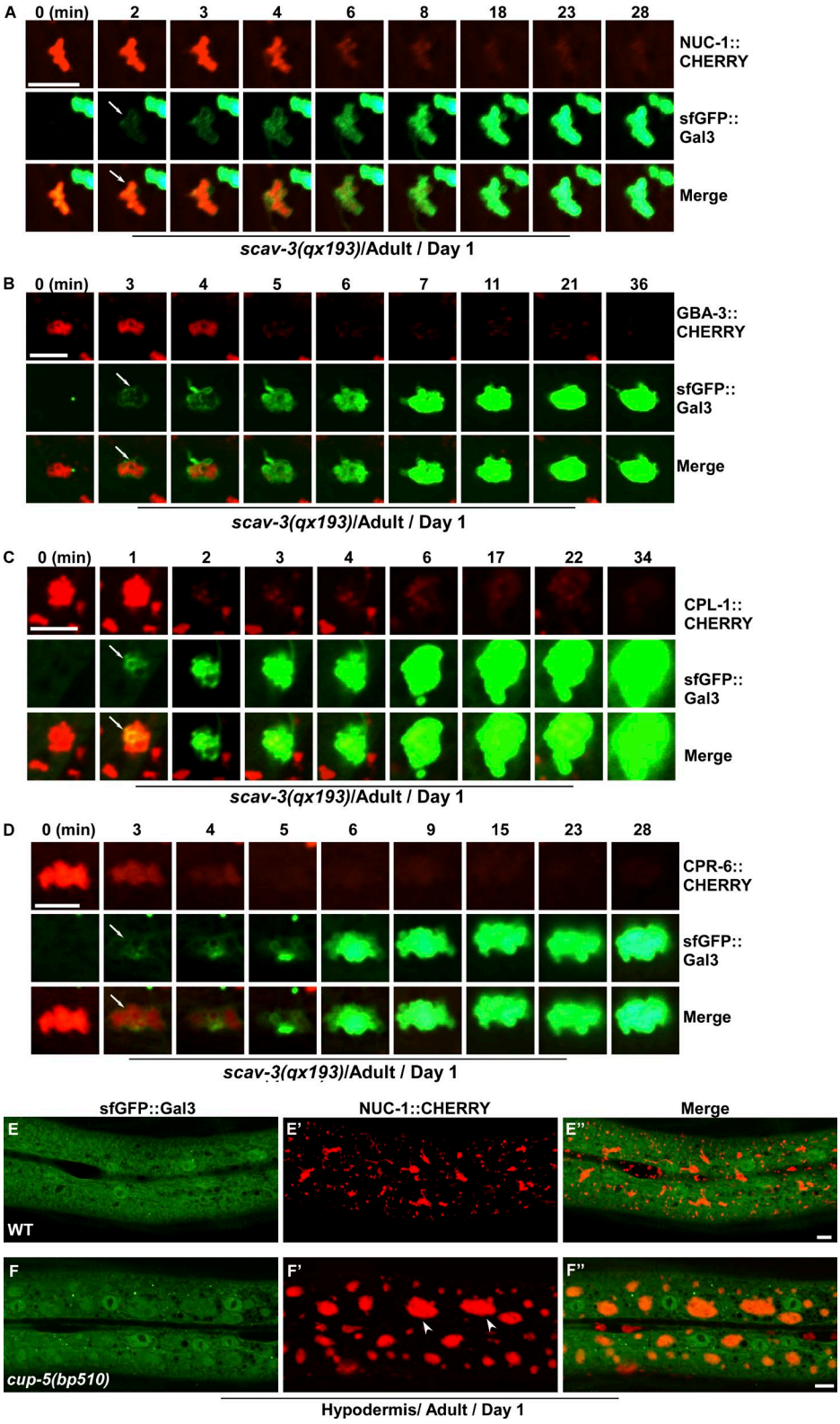

Figure 6. **Loss of *scav-3* causes leakage of lysosome luminal hydrolases.** (A–D) Time-lapse images of lysosomes in *scav-3(qx193)* expressing sfGFP::Gal3 and NUC-1::mCherry (A), GBA-3::mCherry (B), CPL-1::mCherry (C), or CPR-6::mCherry (D). 0 min represents the time point before initial appearance of sfGFP::Gal3 around the lysosome (arrows). (E–F″) Confocal fluorescent images of the hypodermis in wild-type (WT; E–E″) and *cup-5(bp510)* (F–F″) adults expressing sfGFP::Gal3 and NUC-1::mCherry. Gal3 was diffuse in the cytosol in wild-type and in *cup-5* mutants that contained enlarged lysosomes (arrowheads). Bars, 5 µm.

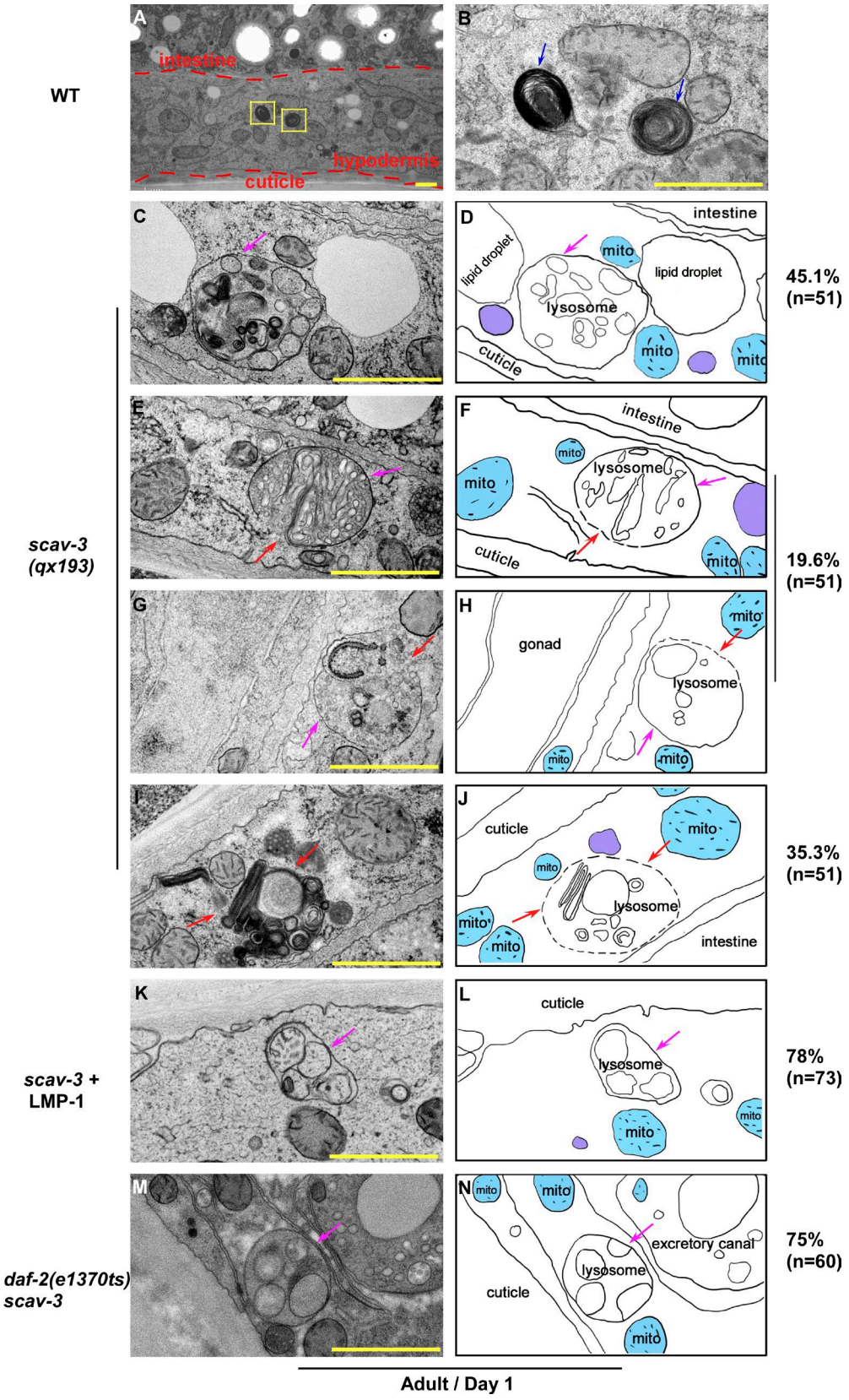

Figure 7. **Loss of *scav-3* causes damage to lysosome membranes.** TEM scans of lysosomes in the hypodermis of wild type (WT; A and B, blue arrows), *scav-3(qx193)* without (C–J) or with LMP-1 expression (K and L), and *daf-2(e1370ts) scav-3* (M and N). Traces of membranes are shown in D, F, H, J, L, and N. The lysosome membrane is indicated by solid or dashed circles, which represent detectable (pink arrows) and undetectable (red arrows) membranes, respectively. The boxed region in A is magnified in B. The percentage of lysosomes with the representative pattern is shown at the right. Bars, 1 µm.

Results

qx193 mutation affects lysosomal morphology and dynamics

We coexpressed the lysosomal DNase II NUC-1 and the lysosomal membrane protein LAAT-1 to visualize lysosomes in live *C. elegans* (Guo et al., 2010; Liu et al., 2012). In wild type, NUC-1 and LAAT-1 labeled both vesicular and tubular structures at embryonic, larval, and adult stages in multiple tissues (Fig. 1, A–A″, C–C″, and E–E″; and Fig. S1, A–C). The vesicular and tubular lysosomes are mobile and undergo a variety of dynamic changes (Figs. 1 J and S1 L). In *qx193*, a recessive mutation generated by γ-irradiation, however, we observed significantly enlarged globular lysosomes (Fig. 1, B–B″, D–D″, and F–F″; and Fig. S1 D). In wild type, 82% and 73% of lysosomes in fourfold embryos and L1 larvae are small, with volumes of 0.02–0.4 μm^3 (Fig. 1, G and H). The mean lysosome volume in embryos and larvae is 0.39 and 0.31 μm^3, respectively (Fig. 1 I). In *qx193* mutants, however, 56% and 44% of lysosomes in fourfold embryos and L1 larvae are big, ranging in volume from 0.4 μm^3 to more than 10.2 μm^3 (Fig. 1, G and H). The mean volumes reached 1.2 and 1.05 μm^3 in embryos and larvae, respectively, which are 2.1 and 2.4 times bigger than in wild type (Fig. 1 I). *qx193* mutants lacked tubular lysosomes at both embryonic and larval stages, whereas tubule-like structures that were much thicker than wild-type tubules were present in *qx193* adults (Fig. 1, B–B″, D–D″, and F–F″; and Fig. S1 D). Thus, both globular and tubular lysosomal structures are affected in *qx193* mutants. In contrast, reporters of ER (GFP::TRAM), Golgi membrane (MANS::GFP), early endosomes (YFP::2xFYVE, HGRS-1::GFP), and recycling endosomes (GFP::RAB-10, GFP::RAB-11, and GFP::RME-1) in *qx193* mutants showed similar patterns to those in wild type, indicating that these intracellular organelles are not affected (Fig. 2). In addition to morphological changes, lysosomes were obviously less dynamic in *qx193* than in wild type (Fig. S1 M). We measured the Pearson's correlation coefficient to compare the colocalization of lysosomes in two time-lapse image frames taken 20 s apart (French et al., 2008). We found that LAAT-1::GFP–labeled lysosomes were more colocalized in *qx193*, resulting in higher Pearson's correlation in *qx193* than in wild type (Fig. 1 J) and indicating that lysosomal dynamics are affected in *qx193*.

qx193 affects SCAV-3, a widely expressed lysosomal membrane protein

We found that *qx193* causes a 648-bp deletion in *scav-3*, which encodes a conserved protein homologous to the human lysosomal integral membrane protein LIMP-2 (Fig. S2, A and L). SCAV-3 and LIMP-2 contain two predicated transmembrane domains and share 76% sequence similarity and 28% sequence identity (Fig. S2 L). Two *scav-3* deletion mutants, *ok1286* and *tm2659*, and seven other alleles of *scav-3* isolated from a forward genetic screen all showed lysosome phenotypes similar to *qx193* (Fig. S2, A–G). We generated a SCAV-3::GFP reporter driven by the *scav-3* promoter and found that it fully rescued the lysosome phenotypes of *qx193* (Fig. S2, H–I″). SCAV-3::GFP is widely expressed during embryonic, larval, and adult stages in various tissues including pharynx, hypodermis, sheath cells, vulva, and tail region (Fig. 3, A–F′). SCAV-3::GFP was not evident in the intestine and was only very weakly expressed in body wall muscle cells, consistent with less severely affected lysosomes in these two cell types in *scav-3(lf)* mutants (Fig. S1, E and F). SCAV-3::GFP labeled both puncta and tubular structures that were positive for NUC-1 and LAAT-1, suggesting that SCAV-3 localizes to lysosomes (Fig. 3, G–H″). SCAV-3(AAA)::GFP, in which the C-terminal leucine-based lysosomal targeting motif (Leu^{516}-Val^{517}-Leu^{518}) was replaced by three alanines, mostly stained plasma membranes, further suggesting that SCAV-3 is a lysosomal membrane protein (Fig. 3, I and J; and Fig. S2 L).

β-GCase is transported to lysosomes in *scav-3* mutants

Human LIMP-2 is an abundant lysosomal membrane protein that performs multiple functions including transporting β-GCase to lysosomes (Reczek et al., 2007). We found that the *C. elegans* β-GCase GBA-3 localized to both vesicular and tubular lysosomes in wild type and appeared in the enlarged lysosomes in multiple *scav-3* mutant strains, including those with deletion mutations that cause large protein truncations and those with missense mutations that abolish lysosomal targeting of SCAV-3 (Fig. 4, A and B; Fig. S1, O–R″; and Fig. S2, J–L; Materials and methods). This suggests that loss-of-function of *scav-3* does not affect lysosomal localization of GBA-3. In addition, GBA-1 (glucosidase), CPL-1 (cathepsin L), CPR-6 (cathepsin B), Y105E8B.9 (β-glucuronidase), and ASM-1 (acid sphingomyelinase) were all transported to lysosomes in *scav-3(qx193)* mutants as in wild type, suggesting that lysosomal targeting of these hydrolases is not affected by loss of *scav-3* function (Fig. 4, C–L).

Loss of *scav-3* causes damage to the lysosome membrane

SCAV-3 contains a large intraluminal loop that is probably highly glycosylated, as in LIMP-2 (Vega et al., 1991). We next investigated whether SCAV-3 may play a structural role to protect the integrity of lysosome membranes. To do this, we expressed GFP fusions of galectin 3 (Gal3) and Gal9 in worms. Gal3 and Gal9 are β-galactoside–binding proteins that bind luminal glycoproteins of endosomes or lysosomes with ruptured membranes and thus detect endosomal or lysosomal damage (Paz et al., 2010; Thurston et al., 2012; Maejima et al., 2013). We found that GFP::Gal3 and GFP::Gal9 were diffuse throughout the cytosol in wild-type worms but accumulated as vesicular and irregular membrane-like structures in *scav-3(qx193)* mutants (Fig. 5, A–G; and Fig. S3, A–B″). The GFP::Gal3 and GFP::Gal9 speckles contained diffuse and faint NUC-1::mCherry, whereas GFP rings were seen surrounding NUC-1 puncta with brighter mCherry fluorescence (Fig. 5, B–B″; and Fig. S3, B–B″, arrows). Similar GFP::Gal3 patterns were observed in *scav-3(qx193)* when lysosomes were labeled by CPL-1::mCherry or CPR-6::mCherry (Fig. S3, C–D″). We performed time-lapse analyses in *scav-3(qx193)* mutants to follow dynamic changes of Gal3 and lysosomes labeled by multiple luminal hydrolases. We found that GFP::Gal3 appeared initially around lysosomes containing bright NUC-1::mCherry, GBA-3::mCherry, CPL-1::mCherry, or CPR-6::mCherry, which was followed by gradual enrichment of GFP with the concomitant loss of mCherry fluorescence (Fig. 6, A–D; and Videos 1, 2, 3, and 4). Collectively, these data suggest that loss of *scav-3* causes damage to lysosome membranes, leading to leakage of the lysosomal hydrolases NUC-1, GBA-3, CPL-1, and CPR-6 into the cytosol and association of cytosolic Gal3 and Gal9 with glycoproteins at the luminal leaflet of lysosomes. Consistent

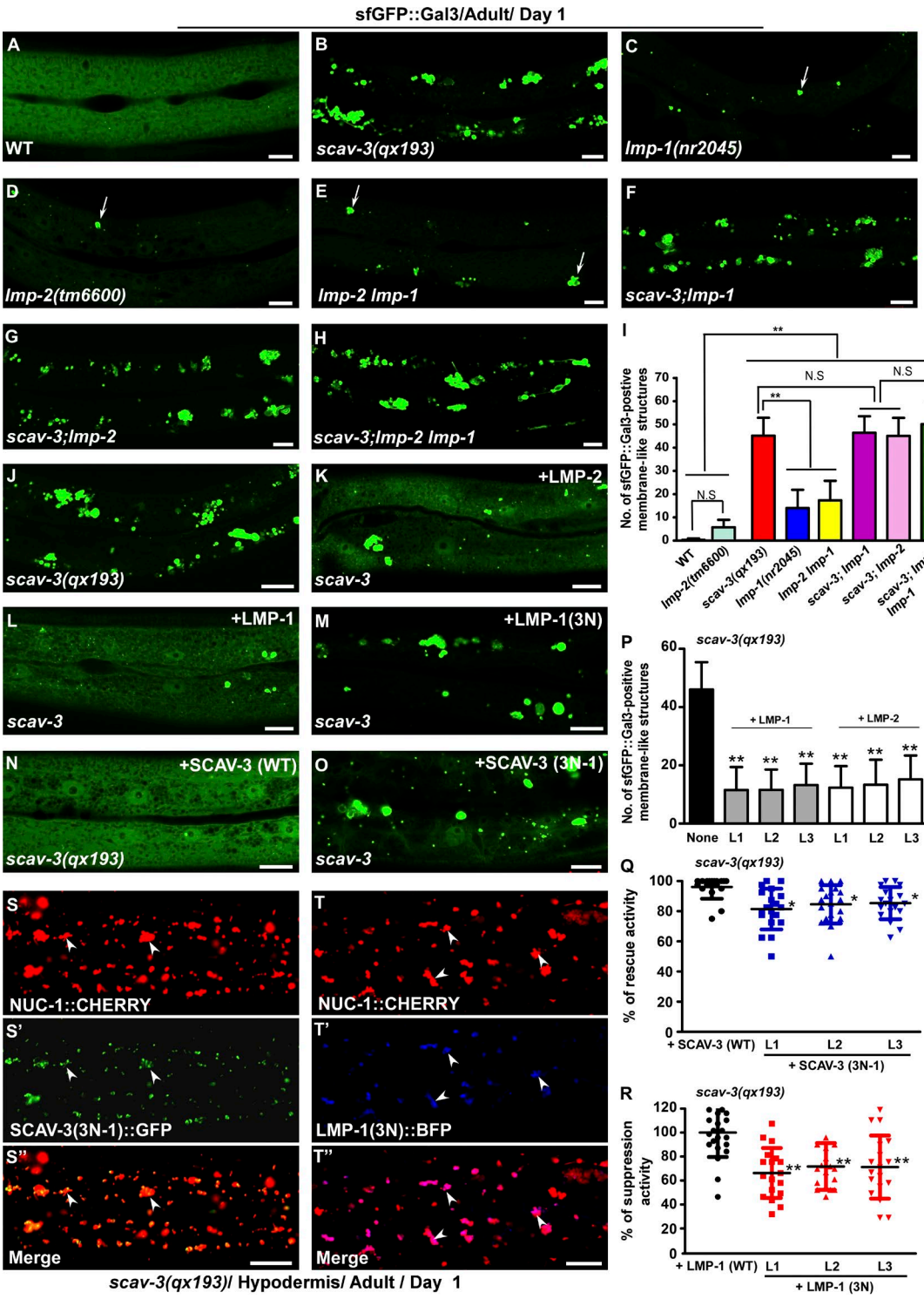

Figure 8. **Overexpression of LMP-1 and LMP-2 suppresses accumulation of damaged lysosomes in *scav-3(lf)*.** (A–H) Confocal fluorescent images of the hypodermis in the indicated strains expressing sfGFP::Gal3. Very few sfGFP::Gal3-positive membrane-like structures were seen in *lmp-1*, *lmp-2*, and *lmp-2 lmp-1* worms (arrows). (J–O) Confocal fluorescent images of the hypodermis in *scav-3(qx193)* expressing sfGFP::Gal3 and LMP-2, wild-type (WT) LMP-1, glycosylation-defective LMP-1, wild-type SCAV-3, or glycosylation-defective SCAV-3. (S–T″) Confocal fluorescent images of the hypodermis in *scav-3(qx193)* expressing NUC-1::mCherry and SCAV-3(3N-1)::GFP or LMP-1(3N)::BFP. SCAV-3(3N-1) and LMP-1(3N) are localized to lysosomes (arrowheads). In panels I and P–R, the number of sfGFP::Gal3-positive membrane-like structures (I and P) or the percentage of rescue or suppression activity (Q and R) was quantified in hypodermal cell *7* (hyp7) of the indicated strains at day 1 of adulthood as shown in A–H and J–O. Data are shown as mean ± SD (I and P) or the distribution of rescue or suppression activity, with black lines representing the mean activity (Q and R). At least 15 animals were scored in each strain. One-way ANOVA with Tukey's posttest was performed to compare all the other datasets with wild type or the nontransgenic control or to compare datasets that are linked by lines. *, $P < 0.05$; **, $P < 0.0001$; N.S., no significance. Bars, 10 µm.

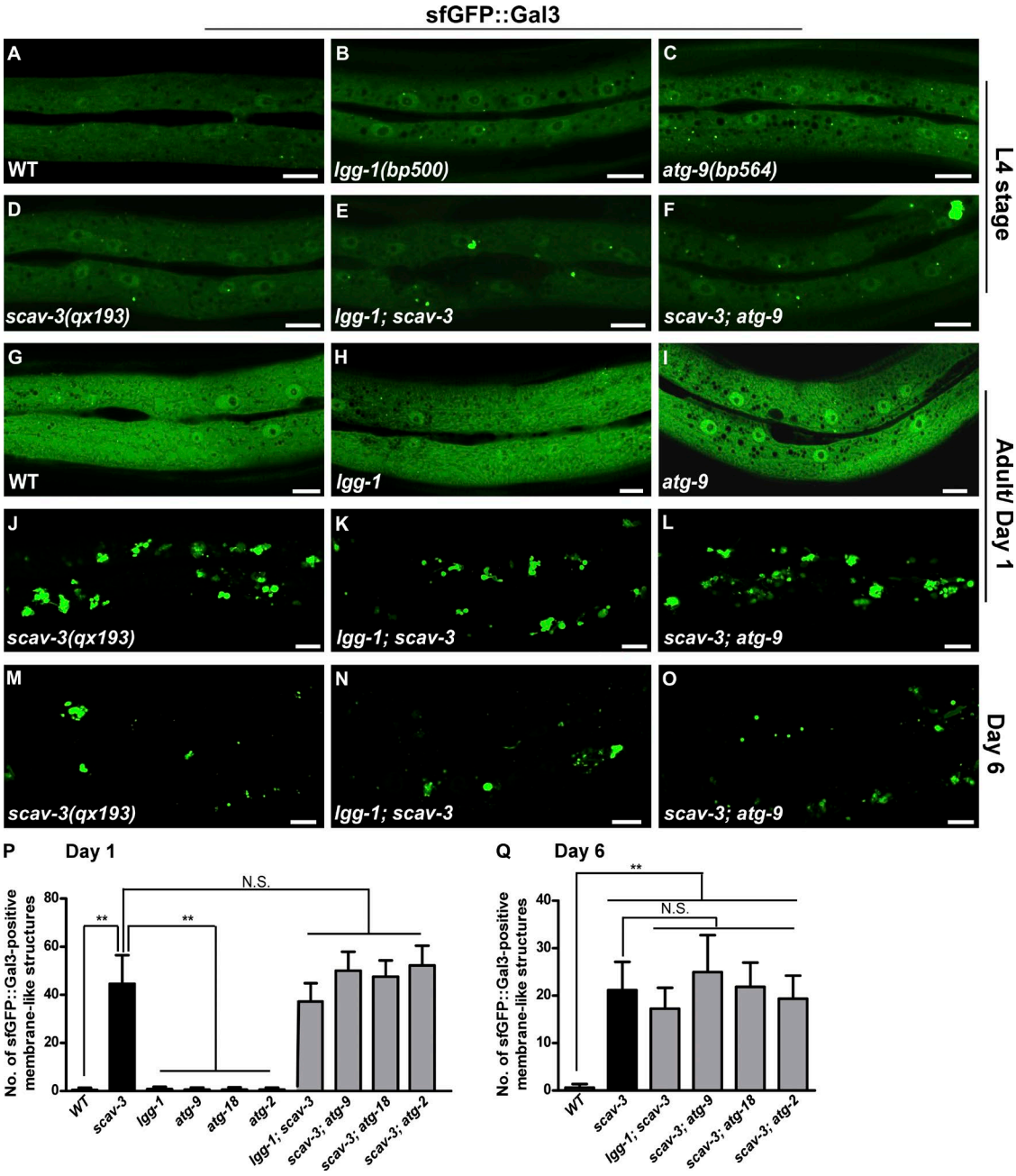

Figure 9. **The number of sfGFP::Gal3-positive damaged lysosomes in *scav-3(qx193)* is not affected by mutations in autophagy genes.** (A–O) Confocal fluorescent images of the hypodermis in the indicated strains expressing sfGFP::Gal3 at L4 stage (A–F) and day 1 (G–L) and day 6 (M–O) of adulthood. (P and Q) The number of sfGFP::Gal3-positive membrane-like structures was quantified in hypodermal cell *7* (hyp7) of the indicated strains as shown in A–O. Data are shown as mean ± SD. At least 15 worms were scored in each strain at each stage. One-way ANOVA with Tukey's posttest was performed to compare datasets that are linked by lines. **, P < 0.0001; N.S., no significance; WT, wild type. Bars, 10 µm.

with leakage of luminal contents after membrane damage, we found that 44–47% of lysosomes in *scav-3(qx193)* contained very weak NUC-1–, CPL-1–, or CPR-6–mCherry, whereas 100% of wild-type lysosomes had bright mCherry fluorescence (Figs. 5 H and S3 E). Moreover, GFP::Gal3-positive structures in *scav-3(qx193)* contained faint or undetectable NUC-1::mCherry or CPL-1::mCherry, whereas GFP::Gal3 was absent from lysosomes with bright mCherry fluorescence (Figs. 5 I and S3 F). Furthermore, GFP::Gal3-positive structures in *scav-3(qx193)* were not stained by LysoTracker red, indicating loss of interior acidity after lysosomal membrane damage (Fig. 5, J–L).

To further examine lysosome damage in *scav-3(lf)*, we performed transmission electron microscopy (TEM) analyses. In wild-type worms, lysosomes appeared as dense, spherical, membrane-enclosed vesicles (Fig. 7, A and B). In *scav-3(qx193)*, however, we observed three types of abnormal lysosome that were not seen in wild type. First, we found significantly enlarged membrane-bound vesicles that were filled with membranous and granular contents (Fig. 7, C and D; 45.1%, $n = 51$), suggesting accumulation of undigested cargo in lysosomes. Second, we observed large vesicular structures that contained similar cargo but had clear membrane damage (Fig. 7, E–H, red arrows; 19.6%,

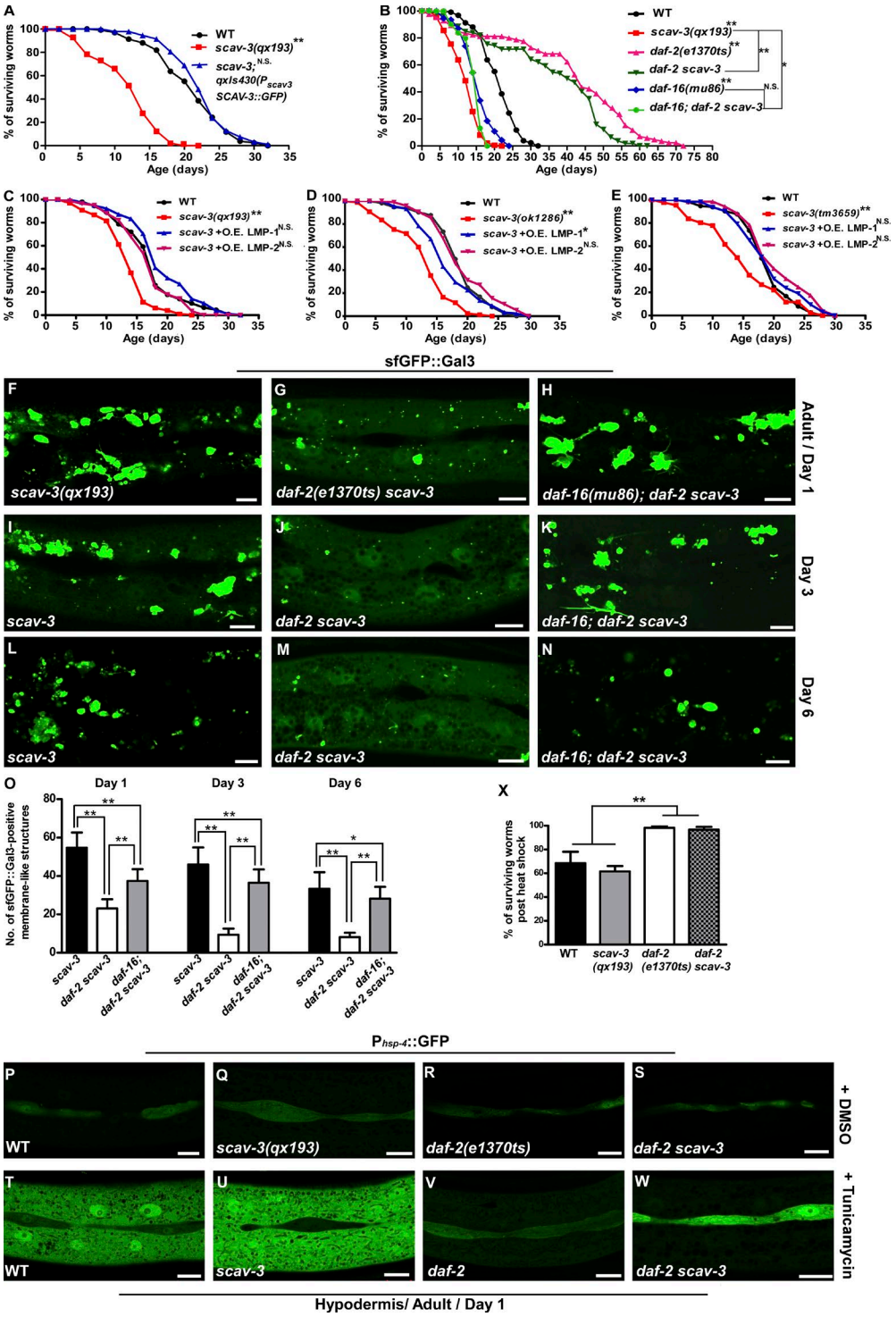

Figure 10. **Inhibition of insulin/IGF-1 signaling suppresses lysosome damage and extends the shortened lifespan of *scav-3(qx193)*.** (A–E) Lifespan analyses in the indicated strains. More than 100 worms were quantified in each strain. Kaplan–Meier method followed by log-rank test was performed to compare all the other datasets with wild type (WT) or those that are linked by lines. *, $P < 0.05$; **, $P < 0.0001$; N.S., no significance. (F–N) Confocal fluorescent images of the hypodermis in the indicated strains expressing sfGFP::Gal3 at day 1 (F–H), day 3 (I–K), and day 6 (L–N) of adulthood. Animals were cultured and examined at 25°C, the nonpermissive temperature of the *daf-2(e1370ts)* mutation. (O) The number of sfGFP::Gal3-positive membrane-like structures was quantified in hypodermal cell *7* (hyp7) of the indicated strains as shown in F–N. Data are shown as mean ± SD. At least 15 worms were scored in each strain for each stage or condition. Two-way ANOVA with the Bonferroni posttest was performed to compare datasets that are linked by lines. *, $P < 0.05$; **, $P < 0.001$. (P–W) Confocal fluorescent images of the hypodermis in the indicated strains expressing $P_{hsp\text{-}4}$GFP treated with DMSO (P–S) or tunicamycin (T–W). (X) The survival of worms after heat-shock treatment was quantified in the indicated strains. At least 100 worms were scored in each experiment, and three independent experiments were performed. Data are shown as mean ± SD. One-way ANOVA with Tukey's posttest was performed to compare datasets that are linked by lines. **, $P < 0.0001$. Bars, 10 µm.

$n = 51$). Finally, we saw aggregation of dense granules and membranous structures reminiscent of undigested cargo in the enlarged lysosomes, but very little or no surrounding membranes were detected (Fig. 7, G and H; 35.3%, $n = 51$). These ultrastructural data indicate that loss of *scav-3* function causes damage to lysosome membranes. To further corroborate this, we purified lysosomes from wild type and *scav-3(qx193)* mutants and examined acid phosphatase activity in the lysosome suspension (Fig. S4 P). We observed higher available acid phosphatase activity in the suspension of *scav-3(qx193)* lysosomes than wild type, suggesting that membrane integrity or permeability is affected in *scav-3(qx193)* lysosomes (Fig. 5 M). Collectively, these data indicate that loss of *scav-3* function affects lysosome integrity and function, causing cargo accumulation and membrane damage.

Lysosome membrane integrity is not severely affected by loss of LMP-1 and LMP-2

LAMPs are the most abundant glycoproteins on the lysosome membrane and are thought to play a protective role against lysosomal hydrolases (Eskelinen, 2006). *C. elegans* has two LAMP-like proteins, LMP-1 and LMP-2 (Kostich et al., 2000; de Voer et al., 2008). LMP-1 was widely distributed but enriched in the intestine and pharynx, whereas LMP-2 expression appeared to be restricted to the intestine (Fig. 3, K–T). In contrast to the predominantly lysosomal localization of SCAV-3, both cell surface and intracellular distribution of LMP-1 and LMP-2 were observed (Fig. 3, K–S). Loss of *lmp-1* and *lmp-2* did not affect lysosome morphology, distribution, or dynamics in hypodermis, sheath cells, or body wall muscles but caused enlarged LAAT-1–positive vesicles in the intestine, consistent with previous findings that loss of *lmp-1* affects lysosome-related organelles in the intestine (Fig. S1, G–K and N; Kostich et al., 2000). We found that worms lacking *lmp-1* or *lmp-2* or both contained very few GFP::Gal3-positive structures in hypodermal cells, whereas diffuse GFP::Gal3 was seen in other tissues including pharynx, intestine, and body wall muscle (Fig. 8, A–E and I; and Fig. S3, L–N). Moreover, loss of LMP-1 and LMP-2 either individually or simultaneously did not further increase the number of GFP::Gal3-positive damaged lysosomes in *scav-3(lf)* (Fig. 8, F–I). These data suggest that lysosomal integrity is not severely affected by loss of LMP-1 and LMP-2. In addition, loss of the lysosomal Ca^{2+} channel CUP-5 or the lysosomal amino acid transporters CTNS-1 and LAAT-1 impairs lysosome function, causing accumulation of enlarged lysosomes, but lysosome integrity was not affected in these mutants (Fig. 6, E–F″; and Fig. S4, A–C; Treusch et al., 2004; Liu et al., 2012).

Glycosylation is important for the maintenance of lysosome membrane stability by SCAV-3 and LMP-1

We found that overexpression of LMP-1 or LMP-2, but not CTNS-1 or LAAT-1, greatly reduced the number of GFP::Gal3-positive structures in *scav-3(qx193)* and increased the ratio of lysosomes with intact membranes revealed by TEM (Fig. 7, K and L; Fig. 8, J–L and P; and Fig. S4, D–G). These data suggest that the increased level of LMP-1 and LMP-2 compensates for the loss of SCAV-3 to maintain lysosome membrane integrity. Overexpression of LMP-1, however, did not reverse the abnormal lysosomal morphology and dynamics in *scav-3(qx193)* mutants, suggesting that SCAV-3 has specific effects on membrane stability (Fig. S5, A, B, E, and F). We next investigated whether glycosylation may contribute to the protective role of SCAV-3 and LMP-1. SCAV-3 and LMP-1 contain 10 and five putative glycosylation sites, respectively, among which six and three are conserved in human LIMP-2 and LAMP1 (Fig. S2, L and M). Peptide *N*-glycosidase F (PNGase F) treatment, which removes both mature and immature N-linked oligosaccharides, greatly reduced the apparent molecular weight of SCAV-3, suggesting that SCAV-3 is highly glycosylated (Fig. S4 M). PNGase F treatment also removed several high molecular mass bands of LMP-1 (Fig. S4 N). Mutation of each individual glycosylation site of SCAV-3 did not affect protein targeting or rescue activity (not depicted), whereas in SCAV-3 mutants, the lack of all six of the conserved glycosylation sites (6N) or the three conserved sites at Asn 233, 278, and 456 (3N-2) severely affected protein stability and targeting, causing greatly reduced protein level, diffuse localization, and significantly decreased rescue activity (Fig. S4, H–M and O). This indicates that glycosylation is critical for the protein stability and targeting of SCAV-3. We found that SCAV-3(3N-1), in which the other three conserved glycosylation sites at Asn 53, 80, and 118 were replaced by Ala, was expressed at a level similar to the wild-type protein. In the absence of PGNase F treatment, the apparent molecular weight of SCAV-3(3N-1) was slightly lower than that of the wild-type protein, which suggests that glycosylation is partially affected (Fig. S4 M). SCAV-3(3N-1) localized to lysosomes but did not completely rescue the lysosome integrity defect in *scav-3(qx193)* mutants, suggesting that glycosylation may contribute to the protection of lysosome membranes by SCAV-3 (Fig. 8, N, O, Q, and S–S″). Mutations in Asn 27, 50, and 60 of LMP-1 [LMP-1(3N)] did not obviously affect protein expression or targeting but may impair glycosylation (Fig. 8, T–T″; and Fig. S4 N). Compared with LMP-1, overexpression of LMP-1(3N) was significantly less effective at suppressing the lysosome damage caused by *scav-3(lf)*, suggesting that glycosylation is important for the protection of lysosome integrity by LMP-1 (Fig. 8, L, M, and R).

Lysosome damage in *scav-3(qx193)* is not affected in autophagy-defective mutants

In cultured mammalian cells, damaged lysosomes caused by lysosomotropic agents or light-activated photosensitizers are cleared through autophagy (Hung et al., 2013; Maejima et al., 2013). We examined lysosome damage in wild-type and *scav-3(lf)* worms that carry mutations in autophagy genes including *lgg-1*, *atg-2*, *atg-9*, and *atg-18* (Tian et al., 2010). We found that GFP::Gal3 was diffuse in autophagy-defective mutants, as in wild-type, indicating that loss of autophagy genes does not cause lysosome damage (Fig. 9, A–C, G–I, and P). Moreover, the number of GFP::Gal3-positive structures in *scav-3(lf)* mutants was not altered by mutations in autophagy genes (Fig. 9, D–F, J–L, and P). We observed that the GFP::Gal3-positive damaged lysosomes appeared in adults but not embryos or larvae of *scav-3(lf)*, and the size and number gradually reduced as the worms grew, resulting in far fewer GFP::Gal3-positive structures at day 6 of adulthood than day 1 (Fig. 9, D, J, M, P, and Q). Mutations in autophagy genes did not affect this reduction in GFP::Gal3-positive damaged lysosomes in *scav-3(lf)* (Fig. 9, M–O and Q). Thus, the appearance and persistence of damaged lysosomes caused by loss of *scav-3* are not altered in autophagy-defective mutants.

Loss of *scav-3* causes shortened lifespan

We found that loss of *scav-3* function caused significantly shortened adult lifespan. *scav-3(qx193)* mutants, which developed normally through embryonic and larval stages, had a mean lifespan of 12.1 d, which is 42% shorter than wild type (20.8 d; Fig. 10 A). The maximum lifespan of *scav-3(qx193)* was also shorter than wild-type worms (Fig. 10 A). The shortened lifespan phenotype of *scav-3(qx193)* was efficiently rescued by expression of SCAV-3::GFP, leading to a restored mean lifespan of 22.5 d (Fig. 10 A). These data suggest that lysosome integrity and function maintained by SCAV-3 is important for longevity.

Reducing insulin/IGF-1 signaling suppresses lysosome damage and extends the lifespan of *scav-3(lf)* mutants

Inhibiting insulin/IGF-1 signaling extends the *C. elegans* lifespan. Decreased activity of the insulin/IGF-1 receptor DAF-2 leads to significantly extended lifespan, which requires the function of DAF-16, a FOXO transcription factor (Murphy and Hu, 2013). We found that *daf-2(e1370ts)*, a temperature-sensitive (ts) mutation of *daf-2* that lives twice as long as wild-type worms, significantly extended the lifespan of *scav-3(qx193)* (Fig. 10 B). The lifespan extension of *daf-2 scav-3* was completely suppressed in *daf-16;daf-2 scav-3* triple mutants, which exhibited a shortened lifespan similar to *scav-3(lf)* and *daf-16(lf)* (Fig. 10 B). This indicates that DAF-16 mediates the lifespan extension of *scav-3(lf)* by *daf-2(lf)*. *daf-2(e1370ts) scav-3(qx193)* worms contained greatly reduced numbers of GFP::Gal3-positive structures at both early and late stages of adulthood (Fig. 10, F–O). Moreover, many more lysosomes with intact membranes were observed by TEM in *daf-2(e1370ts) scav-3(qx193)* worms (75%, $n = 60$; Fig. 7, M and N). These data suggest that inhibiting insulin/IGF-1 signaling suppresses lysosome damage in *scav-3(lf)*. The Gal3::GFP-positive structures, which decreased significantly in *daf-2(e1370ts) scav-3(qx193)*, reappeared in *daf-16;daf-2scav-3*, indicating that *daf-16* is required for suppression of lysosome damage by *daf-2(lf)* (Fig. 10, H, K, N, and O). In contrast, inactivation of HSF-1 or SKN-1, the two transcription factors that are also regulated by insulin/IGF-1 signaling, had no effect on the suppression of lysosome damage by *daf-2(e1370ts)* (Fig. S5, L–Q). Collectively, these data suggest that inhibiting insulin/IGF-1 signaling suppresses lysosome damage through the DAF-16 transcription factor, leading to lifespan extension of *scav-3(lf)*. Overexpression of LMP-1 and LMP-2, which led to a significant reduction in damaged lysosomes in *scav-3(lf)*, also restored the lifespan of *scav-3(lf)*, further emphasizing that maintenance of lysosome integrity is important for longevity (Fig. 10, C–E). Inhibition of lysosomal damage by overexpression of LMP-1 and LMP-2 was not affected by loss of *daf-16*, suggesting that the effect of LMP-1 and LMP-2 is independent of or bypasses the activity of DAF-16 (Fig. S5, R–U).

Reducing insulin/IGF-1 signaling leads to increased resistance to a wide variety of stresses. We found that tunicamycin treatment induced a strong ER unfolded protein response, indicated by $P_{hsp\text{-}4}$GFP expression in wild type and *scav-3(qx193)* but not in *daf-2(e1370ts)* or *daf-2(e1370ts) scav-3(qx193)* (Fig. 10, P–W; Calfon et al., 2002). Moreover, significantly more *daf-2(e1370ts)* and *daf-2(e1370ts) scav-3(qx193)* worms survived after heat-shock treatment than wild type or *scav-3(qx193)*, indicating increased thermotolerance (Fig. 10 X). These data suggest that inhibiting insulin/IGF-1 signaling increases stress resistance in *scav-3(lf)*. Reduced DAF-2 activity or overexpression of LMP-1 led to decreased lysosome volume in *scav-3(qx193)* adults but did not alter the abnormal lysosomal morphology and dynamics in *scav-3(qx193)* larvae, suggesting that lysosome function is not fully restored in these animals (Fig. S5, A–K).

Discussion

SCAV-3/LIMP-2 maintains lysosome integrity and dynamics

The lysosome membrane is the physical barrier that separates the luminal acidic milieu from the cytoplasmic environment, thus protecting cellular constituents from unwanted degradation. The mechanisms that preserve lysosomal membrane remain unclear. Here we found that SCAV-3, the *C. elegans* homologue of human LIMP-2, plays an essential role in maintaining lysosome integrity. Overexpression of LMP-1 or LMP-2 efficiently suppressed lysosome damage caused by loss of *scav-3*, indicating that *C. elegans* LAMPs can act as structural proteins and substitute for the function of SCAV-3 in maintaining the stability of lysosome membranes. In contrast, loss of other lysosome membrane proteins, such as the calcium channel CUP-5 and the amino acid transporters LAAT-1 and CTNS-1, impairs lysosome function and causes enlargement of lysosomes but has no effect on membrane integrity, which further suggests that SCAV-3 plays a specific role in preserving lysosomal membrane stability.

Extensive glycosylation in the luminal portion of abundant lysosomal membrane proteins has been suggested to perform a protective role by forming a continuous carbohydrate layer at the luminal leaflet (glycocalyx) to prevent membrane damage by the lysosomal hydrolases (Lewis et al., 1985; Fukuda, 1991). Expression of SCAV-3(3N-1) and LMP-1(3N), which contained mutations in the conserved glycosylation sites and caused partially impaired glycosylation, did not affect protein stability or targeting but led to reduced preservation of lysosomal membrane stability. This suggests that glycosylation of SCAV-3 and LMP-1 may contribute to the formation of the glycocalyx that protects lysosomal membranes from the damage by luminal hydrolases. However, mutations that abolished all six of the conserved glycosylation sites (6N), or the three conserved sites at Asn 233, 278, and 456 (3N-2) of SCAV-3, severely affected protein stability and targeting, thus precluding us from further analyzing their effects on membrane protection. More in-depth analyses will therefore be needed to demonstrate the function of SCAV-3 in glycocalyx formation. The accumulation of damaged lysosomes caused by loss of *scav-3* is more evident in the hypodermis, where SCAV-3 is highly expressed, but LMPs are not. Future studies are also needed to identify cellular mechanisms responsible for the cell type–specific requirement for SCAV-3 and to reveal the function of LMPs in protecting lysosome membrane integrity.

We found that *C. elegans* lysosomes are mobile and undergo a variety of dynamic changes, a process that requires SCAV-3 function. Overexpression of LMP-1 efficiently suppressed membrane damage but not the abnormal morphology or defective dynamics of *scav-3(lf)* lysosomes, suggesting that SCAV-3 may regulate lysosome integrity and dynamics by distinct mechanisms. Future investigations should address the mechanisms by which SCAV-3 functions in these two processes.

Mammalian LIMP-2 was identified as a receptor for transporting β-GCase, the enzyme defective in Gaucher disease, to lysosomes in an mannose 6-phosphate–independent manner (Reczek et al., 2007). In worms, however, lysosomal localization of β-GCase is not affected by loss of *scav-3*, suggesting the involvement of different targeting mechanisms. LIMP-2 deficiency has been implicated in the pathogenesis of Gaucher disease and Parkinson disease because of its role in transporting β-GCase to lysosomes (Gonzalez et al., 2014). Moreover, mutations in *SCARB2*, the gene encoding LIMP-2, have been identified as the cause of action myoclonus–renal failure, a fatal inherited form of progressive myoclonic epilepsy associated with renal failure or neurological symptoms. The underlying pathogenesis, however, remains unclear (Berkovic et al., 2008; Gonzalez et al., 2014). Our findings reveal the essential role of SCAV-3 in the maintenance of lysosomal membrane integrity and dynamics, which may contribute to the pathogenesis of diseases caused by or associated with LIMP-2 deficiency.

Lysosomal membrane stability is modulated by the insulin/IGF-1 signaling pathway and is important for longevity

In *scav-3(lf)* mutants, abnormal lysosomal morphology and dynamics were observed from embryonic to adult stages, whereas damaged lysosomes did not appear until adulthood. This suggests that lysosomes may enter a damage-prone stage before becoming ruptured. We found that inhibition of insulin/IGF-1 signaling efficiently suppressed lysosome damage in *scav-3(lf)* in a DAF-16–dependent manner, indicating that the *DAF-2/IGFR-DAF-16/FOXO* pathway plays an important role in modulating lysosomal membrane stability. We found that down-regulation of *daf-2* signaling increases stress resistance in *scav-3(lf)*. Down-regulated *daf-2* signaling may alleviate the stress on *scav-3(lf)* lysosomes by reducing lysosomal substrate loading, thus maintaining membrane stability. In addition, the insulin/IGF-1 pathway may control expression of lysosomal genes that increase the physical stability of membranes or promote cargo digestion, thus stabilizing the damage-prone lysosomes.

Lysosomes are the final destinations of damaged cellular structures and proteins that accumulate during aging. We found that SCAV-3 is essential for maintaining lysosome integrity and normal adult lifespan, and that both lysosomal damage and shortened lifespan in *scav-3(lf)* are rescued or extended by reduced *daf-2* signaling or LMP-1 and LMP-2 overexpression. This suggests that lysosome integrity is an important component in lifespan regulation. The suppression of lysosome damage by *daf-2* mutation is dependent on DAF-16 but not HSF-1 or SKN-1, indicating specific roles of DAF-16 in this process. Given the evolutionary conservation of the insulin/IGF-1 signaling pathway in metazoans, similar mechanisms may be used in mammals to modulate lysosome integrity in longevity.

Lysosomes damaged by lysosomotropic agents or light-activated photosensitizers in cultured mammalian cells are cleared by autophagy, leading to recovery of low pH and degradation capacity (Hung et al., 2013; Maejima et al., 2013). In *scav-3(lf)* mutants, however, appearance and disappearance of GFP::Gal3-positive damaged lysosomes were unchanged in autophagy-defective mutants. It is conceivable that loss of *scav-3* may affect autophagic removal of damaged lysosomes because of the lack of healthy lysosomes. Alternatively, autophagy-independent mechanisms may be involved. Future investigations should address whether and how autophagy-dependent and/or -independent mechanisms regulate clearance of damaged lysosomes in vivo.

Materials and methods

C. elegans strains

Strains of *C. elegans* were cultured and maintained using standard protocols (Brenner, 1974). The N2 Bristol strain was used as the wild-type strain except in polymorphism mapping, in which Hawaiian strain CB4856 was used. The following strains were used in this work: linkage group (LG) I: *hsf-1(sy441)*, and *daf-16(mu86)*; LG II: *laat-1(qx42)*, *lgg-1(bp500)*, and *ctns-1(ok813)*; LG III: *daf-2(e1370ts)*, *cup-5(bp510)*, and *scav-3(qx193*, *tm3659*, *ok1286*, *qx232*, *qx237*, *qx260*, *qx266*, *qx267*, *qx271*, *qx281)*; LG V: *atg-9(bp564)*, *atg-18(gk378)*, and *zcIs4*; and LG X: *atg-2(bp576)*, *lmp-2(tm6600)*, and *lmp-1(nr2045)*. daf-2(e1370ts) was maintained at 20°C. L4 larvae were moved to 25°C for 24–144 h before the damaged lysosome phenotype was examined.

Transgenic animals carrying extrachromosomal arrays (*qxEx*) were generated using standard microinjection methods, and genome-integrated arrays (*qxIs*) were obtained by γ-ray irradiation to achieve stable expression from arrays with low copy numbers (Evans, 2005). The reporter strains used in this study are listed as follows: *qxIs354* ($P_{ced\text{-}1}$LAAT-1::GFP), *qxIs257* ($P_{ced\text{-}1}$NUC-1::mmCherry), *qxIs352* ($P_{ced\text{-}1}$LAAT-1::nmCherry), *qxIs430* ($P_{scav\text{-}3}$SCAV-3::GFP), *qxIs439* ($P_{hyp\text{-}7}$GFP::TRAM-1), *qxIs468* ($P_{myo\text{-}3}$LAAT-1::GFP), *qxIs582* ($P_{hyp\text{-}7}$sfGFP::Gal3), *qxIs594* ($P_{myo\text{-}3}$sfGFP::Gal3), *qxIs599* ($P_{vha\text{-}6}$sfGFP::Gal3), *qxIs612* (P_{hsp}NUC-1::sfGFP::mmCherry), *qxEx3928* ($P_{hyp\text{-}7}$MANS::GFP), *qxEx4342* ($P_{hyp\text{-}7}$GFP::RAB-10), *qxEx4345* ($P_{hyp\text{-}7}$GFP::RAB-11), *qxEx7016* [$P_{scav\text{-}3}$SCAV-3(AAA)::sfGFP], *qxEx4274* ($P_{vha\text{-}6}$LAAT-1::GFP), *qxEx7170* ($P_{hyp\text{-}7}$sfGFP::Gal9), *qxEx6312* ($P_{vha\text{-}6}$sfGFP::Gal3), *qxEx6953*, *6966*, *6967* ($P_{hyp\text{-}7}$LMP-1::ceBFP), *qxEx6751*, *6752*, *6758* ($P_{hyp\text{-}7}$LMP-2::ceBFP), *qxEx6975*, *6976*, *6977* ($P_{hyp\text{-}7}$LAAT-1::CeBFP), *qxEx6978*, *6979*, *6980* ($P_{hyp\text{-}7}$CTNS-1::CeBFP), *qxEx7189* ($P_{lmp\text{-}1}$LMP-1::sfGFP), *qxEx7190* ($P_{lmp\text{-}2}$LMP-2::sfGFP), *qxEx6981* (P_{hsp}sfGFP::Gal3), *qxEx7396*, *7397*, *7398* [LMP-1(3N): $P_{hyp\text{-}7}$LMP-1(N27A, N50A, N60A)::CeBFP], *qxEx7399*, *7400*, *7401* [SCAV-3(3N-1): $P_{scav\text{-}3}$SCAV-3(N53A, N80A, N118A)::CeBFP], *qxEx7402*, *7403*, *7404* [SCAV-3(3N-2): $P_{scav\text{-}3}$SCAV-3(N233A, N278A, N456A)::CeBFP], *qxEx7405* [SCAV-3(4N): $P_{scav\text{-}3}$SCAV-3(N53A, N233A, N278A, N456A)::CeBFP], *qxEx7406* [SCAV-3(6N): $P_{scav\text{-}3}$SCAV-3(N53A, N80A, N118A, N233A, N278A, N456A)::CeBFP], *qxEx7407* [SCAV-3(3N-1): $P_{scav\text{-}3}$SCAV-3(N53A, N80A, N118A)::sfGFP], *qxEx7408* [SCAV-3(3N-2): $P_{scav\text{-}3}$SCAV-3(N233A, N278A, N456A)::sfGFP], *qxEx7409* [SCAV-3(4N): $P_{scav\text{-}3}$SCAV-3(N53A, N233A, N278A, N456A)::sfGFP], *qxEx7410* [SCAV-3(6N): $P_{scav\text{-}3}$SCAV-3 (N53A, N80A, N118A, N233A, N278A, N456A)::sfGFP], *qxEx7411* [$P_{scav\text{-}3}$SCAV-3(G279R)::sfGFP], *qxEx7412* [$P_{scav\text{-}3}$SCAV-3(S382F)::sfGFP], and *yqEx632* ($P_{cpl\text{-}1}$CPL-1::mCherry).

We obtained *bIs46* ($P_{vit\text{-}2}$GFP::RME-1) from B. Grant (Rutgers University, New Brunswick, NJ); *opIs334* ($P_{ced\text{-}1}$YFP::2xFYVE) from K.S. Ravichandran (University of Virginia, Charlottesville, VA) and M.O. Hengartner (University of Zurich, Zurich, Switzerland); $P_{hgrs\text{-}1}$ HGRS-1::GFP from R. Legouis (Institute for Integrative Biology of the Cell, Gif-sur-Yvette, France); *kxEx147* ($P_{gba\text{-}3}$GBA-3::mCherry), *kxEx152* ($P_{asm\text{-}1}$ASM-1::mCherry), and *kxEx141* ($P_{cpr\text{-}6}$CPR-6::mCherry) from G. Hermann (Lewis and Clark College, Portland, OR); and *scav-3(tm3659)* from S. Mitani (Tokyo Women's Medical University, Tokyo, Japan).

Isolation, mapping, and cloning of *scav-3*

The *qx193* mutation was isolated through backcrossing the genome-integrated array of LAAT-1::GFP generated by γ-ray irradiation. Other alleles of *scav-3* including *qx232*, *qx237*, *qx260*, *qx266*, *qx267*, *qx271*, and *qx281* were isolated from a forward genetic screen using the abnormally enlarged lysosome phenotype. *qx193* was mapped to the right arm of linkage group III (LG III) between genetic map positions 17.26 [Snp-Y49E10(2)] and 21 (Snp-UCE3-1426) by single nucleotide polymorphism mapping. Transformation rescue experiments were performed, and a DNA fragment containing the *scav-3* gene fully rescued the *qx193* defect. The sequence of the *scav-3* gene was determined in all *scav-3* alleles. *qx193* contains a 648-bp deletion that removes most of exon 5, all of exon 6, and part of exon 7, causing an early stop codon that results in a truncated protein containing the first 346 amino acids. The *ok1286* allele of *scav-3* contains a 1,146-bp deletion and a 2-bp insertion that removes most of the second and third exons and generates an early stop codon, resulting in a truncated protein containing only the first 118 amino acids. The *qx237* and *qx266* alleles contain a G-to-A transition that results in a premature stop codon after Ser 321. *qx271* and *qx281* contain C-to-T mutations that cause a premature stop codon after Arg 372 and substitution of Ser 382 with Phe, respectively. *qx260* contains a G-to-A mutation that results in substitution of Gly 279 with Arg. *qx232* and *qx267* contain G-to-A transitions at the splicing sites located at the boundaries of exon 2 and intron 2 and exon 3 and intron 3, respectively, which cause premature stop codons after Ile 133 and Ile 189. The *tm3659* allele of *scav-3* contains a 694-bp deletion that removes the entire fourth and fifth exons and generates an early stop codon, resulting in a truncated protein containing only the first 238 amino acids. All mutants were backcrossed with N2 animals at least four times before further analyses.

RNAi

The bacteria-feeding protocol was used in RNAi experiments as described before (Kamath and Ahringer, 2003). In *skn-1* RNAi experiments, 30 L1 or L2 larvae were cultured on the RNAi plates, and lysosome damage was examined in adult animals at the same generation because most F1 progeny die because of inactivation of *skn-1*. The DNA sequence that is targeted by the dsRNA in the RNAi experiments is *skn-1* (T19E7; 590–2,157 nt).

LysoTracker staining

Aged adult worms (>50) were soaked in 100 µl LysoTracker red in M9 (1:200; Invitrogen) for 1.5 h at 20°C in the dark. Worms were then transferred to a fresh OP50-seeded NGM plate and allowed to recover at 20°C for 4 h in the dark before examination by fluorescent microscopy.

Microscopy and imaging analysis

Differential interference contrast and fluorescent images were captured with an Axioimager A1 (ZEISS) equipped with epifluorescence (Filter Set 13 for GFP [excitation BP 470/20, beam splitter FT 495, emission BP 503–530] and Filter Set 20 for Cherry [excitation BP 546/12, beam splitter FT 560, emission BP 575–640]) and an AxioCam monochrome digital camera (ZEISS). Images were processed and viewed using Axiovision Rel. 4.7 software (ZEISS). A 100× Plan-Neofluar objective (NA1.30) was used with Immersol 518F oil (ZEISS). Confocal images were captured by an LSM 5 Pascal (ZEISS) inverted confocal microscope with 488-nm (emission filter BP 503–530) and 543-nm (emission filter BP 560–615) lasers, and images were processed and viewed using LSM Image Browser software (ZEISS). All images were taken at 20°C.

To quantify the fluorescence intensity of LMP-1::sfGFP, 15 images were taken of each cell type with equal exposure time and quantified using ImageJ 1.42q (National Institutes of Health).

Spinning-disk time-lapse recording

L1 larvae or adult worms 24 h after the L4/adult molt were mounted on agar pads in M9 buffer with 5 mM levamisole, which prevents animals from moving but does not affect the hypodermis. Fluorescent images were captured using a 100× objective (CFI Plan Apochromat Lambda; NA 1.45; Nikon) with immersion oil (type NF) on an inverted fluorescence microscope (Eclipse Ti-E; Nikon) with a spinning-disk confocal scanner unit (UltraView; PerkinElmer) with 488-nm (emission filter 525 [W50]) and 561-nm (dual-band emission filter 445 [W60] and 615 [W70]) lasers. To follow lysosome dynamics, images were captured every 2 s (wild type) or 5 s (*scav-3(qx193)*, *daf-2 scav-3*, and *scav-3*+LMP-1) for 5 min. To examine dynamic changes in worms coexpressing sfGFP::Gal3 and mCherry fusions of NUC-1, GBA-3, CPL-1, or CPR-6, images were captured every 1 min for 1–3 h. The collected images were viewed and analyzed using Velocity software (PerkinElmer).

Quantification of lysosome dynamics by Pearson's correlation coefficient

Time-lapse images of L1 larvae expressing LAAT-1::GFP or NUC-1::mCherry were captured by spinning-disk microscopy. The colocalization of two frames taken 20 s apart was analyzed by Velocity software. At least 10 independent videos were followed and quantified in each strain. Selected images from the representative videos are shown in Figs. 1 J, S1 N, and S5 F.

Quantification of lysosome volume

Fluorescent images of embryos, larvae, or adults expressing LAAT-1::GFP or NUC-1::mCherry in 10–15 *z*-series (0.5 µm/section) were captured by spinning-disk microscopy. Serial optical sections were analyzed, and the volume of LAAT-1::GFP– or NUC-1::mCherry–positive lysosomes was quantified by Velocity software. At least 10 animals were quantified in each strain at each stage.

Quantification of damaged lysosomes

To examine damaged lysosomes, fluorescent images were captured using an Axioimager A1 microscope equipped with epifluorescence and an AxioCam monochrome digital camera or an LSM 5 Pascal inverted confocal microscope with equal exposure time. Damaged lysosomes were quantified by scoring the number of sfGFP::Gal3-positive membrane-like structures in hypodermal cell 7 that covers the whole midbody of the worm. Leakage of lysosomal hydrolases was quantified by scoring the percentage of lysosomes that contained strong mCherry fluorescence and were negative for sfGFP::Gal3 (intact) and those that contained faint mCherry fluorescence and were positive for sfGFP::Gal3 (damaged) in wild type and *scav-3(qx193)* expressing mCherry fusions of the lysosomal hydrolases NUC-1, CPL-1, or CPR-6. At least 15 animals were scored in each strain at each stage.

The fluorescence intensity of lysosomes in *scav-3(qx193)* coexpressing sfGFP::Gal3 and NUC-1::mCherry or CPL-1::mCherry or stained by LysoTracker red was quantified by linescan analysis. Fluorescent images of lysosomes were captured by spinning-disk microscopy. A line of 6 to 12 µm in length was manually drawn through a lysosome containing bright GFP or mCherry fluorescence (dashed lines in Fig. 5 [I and L] and Fig. S3 F), and the fluorescence pixel intensity along the line was calculated by Velocity software.

Lifespan assay

Lifespan assays were performed at 20°C as described previously (Hansen et al., 2005). In brief, worms at the L4 stage (day 0, >100) were placed on NGM plates seeded with OP50, with 10 worms per plate. The animals were transferred to new plates when their progeny grew

up to the L3 stage, and dead animals were counted every 2 d. Animals that crawled off the plate, exploded, bagged, or became contaminated were discarded.

Tunicamycin and heat-shock treatment

Worms at day 1 after L4 were treated with tunicamycin at 5 µg/ml. The expression of $P_{hsp\text{-}4}$GFP was examined 10 h after treatment to assess the ER unfolded protein response. To examine thermotolerance, worms (>100) at day 1 of adulthood were incubated at 37°C for 2.5 h and recovered at 20°C for 12 h before survival rate was quantified.

Lysosome purification and examination of acid phosphatase activity

Lysosomes were purified from *C. elegans* at day 1 of adulthood using a Lysosome Isolation kit (LYSISO1; Sigma-Aldrich) as described previously with minor modifications (Liu et al., 2012). In brief, the crude lysosomal fraction was purified on a density gradient built up with Optiprep Density Gradient Medium Solution and Sucrose (bottom to top: 27, 19, 16, and 8%). After centrifugation, the enrichment of lysosomes in the different fractions (bottom to top: B1–4) was determined by examining the processing of cathepsin using anti–CPL-1 antibodies after normalization to the same total protein concentration. The purified lysosome fraction (B3; Fig. S4 P) from wild type and *scav-3(qx193)* was normalized to the same total protein concentration and suspended in the extraction buffer provided in the Lysosome isolation kit. The available acid phosphatase activity in the lysosome suspension was examined using an acid phosphatase assay kit (CS0740; Sigma-Aldrich). Samples were incubated at 25°C for 30 min, and the reactions were stopped by the addition of 0.5 N NaOH before measurement of the absorbance at 405 nm. Activities were compared with the total activities obtained in the presence of 0.1% Trion X-100 and are presented as a percentage of the total activity in Fig. 5 M. At least five independent experiments were performed in each strain, and the mean percentage of total activity is shown.

Examination of glycosylation

Adult worms expressing wild-type or mutant versions of SCAV-3::GFP or LMP-1::BFP that lack multiple glycosylation sites were lysed by several cycles of freeze-thawing. The resulting lysates were denatured before incubating with PNGase F for 1 h at 37°C following the manufacturer's instructions (New England BioLabs, Inc.). The proteins were resolved by SDS-PAGE and revealed by anti–SCAV-3 or anti–LMP-1 antibodies.

TEM analysis

Adult *C. elegans* (day 1 of adulthood) were rapidly frozen using a high-pressure freezer (EM PACT2; Leica Biosystems). Freeze-substitution was performed in anhydrous acetone containing 1% osmium tetroxide. The samples were kept sequentially at −90°C for 72 h, −60°C for 8 h, and −30°C for 8 h and were finally brought to 20°C for 10 h in a freeze-substitution unit (EM AFS2; Leica Biosystems). The samples were washed three times (1 h each time) in fresh anhydrous acetone and were gradually infiltrated with Embed-812 resin in the following steps: resin/acetone 1:3 for 3 h, 1:1 for 5 h, 3:1 overnight, and 100% resin for 4 h. Samples were then kept overnight and embedded at 60°C for 48 h. The fixed samples were cut into 70-nm sections with a microtome EM UC6 (Leica Biosystems) and electron stained with uranyl acetate and lead citrate. Sections were observed with a JEM-1400 (JEOL) operating at 80 kV.

Statistical analysis

The SD was used as *y*-axis error bars for bar charts plotted from the mean value of the data. Data derived from different genetic backgrounds were compared by Student's two-tailed unpaired *t* test, one-way analysis of variance (ANOVA) followed by Tukey's post-test, two-way ANOVA followed by Bonferroni post-test, or Kaplan–Meier method followed by log-rank test as indicated in the figure legends.

Table 1. **Primers used for plasmid construction**

Primer	Sequence (5′ to 3′)
PWZ853	GTGGTTTCCGACTGTTGT
PWZ855	GAAAAGTTCTTCTCCTTTACTCATTGCCAAAACTGCGTTCTCGTC
PHWD478	ATGAGTAAAGGAGAAGAACTTTTCAC
PWZ512	GAAACGCGCGAGACGAAAGGGCCCGT
PWZ854	TCCGACTGTTGTTAGGTG
PPFG199	AAGGGCCCGTACGGCCGACTAGTAGG
PDFZ623	CGGGTACCGGATCGCGAGGAACGCGTATGGTGAGCAAGGGCGAGGAGC
PDFZ624	GCGATATCTGATCCTCCACCTCCTGATCCTCCACCTCCCTTGTACAGCTCG TCCATGCCG
PWZ862	CGGCTAGCATGTTGAAAAAAGCGCCGTGC
PDFZ721	GCACGCGTTGCCAAAACTGCGTTCTCGTCTTG
PWZ895	GCAAGCTTGTGGTTTCCGACTGTTGTTAGGTG
PWZ896	GCCTGCAGTTTACTGAAAAAAAAAAAATTCAATTTCGC
PYL379	ACGTGCTGCGGCGGAGGATGAGGACGAAGAGCCTGCGCAAG
PYL380	TCTCCGCCGCAGCACGTCCGTACTCTTCTTCGTCGGATTG
PYTX95	CGGCTAGCATGGGAAAACGCAATTTCTA
PYTX96	CGGGTACCTTCTTCATCAAAATCTACCG
PYJ45	GGGGTACCTTAATTTTTCTTCTTCGAATCG
PBL727	CGGGTACCATTTTTCTTCTTCGAATCGCTC
PDFZ627	CGGAGCTCTTATATCATGGTATATGAAGCACTG
PDFZ628	GCGATATCATGGCAGACAATTTTTCGCTCCATG
PDFZ898	CGGATATCATGGCCTTCAGCGGTTCCCAG
PDFZ899	CGGATATCCTATGTCTGCACATGGGTCAG
PSZ46	CGGCTAGCATGTTGAAATCGTTTGTCATC
PSZ47	CGGCTAGCGACGCTGGCATATCCTTGTCTC
PXCW192	GCGGTACCATGAAACAAAAATGCACCTG
PXCW193	GCGGTACCAAATCGCTCAATTGAAGATGTC
PPFG227	GGGCTAGCATGAGTTTCCCGGTGGCATTTTTG
PPFG228	GGGCTAGCTAGTCATGTACAATAATAGGTTCCG
PBL516	GCGGTACCATGAAGACGGGCGGTTTGAGTG
PBL515	CGGGTACCCTAATCGGAGTCGTCTTGTGA
PBL520	GCCTGCAGGAGAAGACCACCCAATAGATGAC
PBL521	GCCCCGGGAGTTCAATTGTGTAGAATGAGTC
PDFZ989	CGCTGCAGCAATGAAATGTGCATTTCTAGTC
PDFZ990	CGCCCGGGCTGTTGATAATAATAAAATTGATAAG
PYL365	GATTAACAGAACCGATGGACAATTGTTCAGTCCGATG
PYL366	TCGGTTCTGTTAATCATTCGTGCGTATTTAGTATCC
PYL367	ATCTATTCAATCCACACTTCTACAACTCACCAATG
PYL368	TGGATTGAATAGATAGACACGTGGATTGCCGGCTTG
PWZ985	GCGAGCTCTAATTAAGCTTGTGACCCAGTTTG
PYL405	GCCTGCAGGTGGTTTCCGACTGTTGTTAGGTG
PDFZ999	CGCCCGGGTTTACTGAAAAAAAAAAATTCAATTTCGC
PDFZ1079	CGAAGCTGGTACAGAGGTACCGAATGCAATGAC
PDFZ1080	TACCAGCTTCGTCGCGTGTGTAGCCGAGAAAATC
PDFZ1081	GTTCGCCGTGACAAATGTTGATGGAATCCTTAAAAG
PDFZ1082	TCACGGCGAACATCCAAATATTCAACTGCATTG
PDFZ1083	TGACGCTGATACCCGAGTATTCTATAAAAATC
PDFZ1084	TATCAGCGTCAGCAAATCTATGATAGACCTTC
PDFZ1087	GCAAGCTGGAACAACAGACGGAATATACGAAG
PDFZ1088	TTCCAGCTTGCTGAAGAAAAATCAATATTTTG
PDFZ1091	GATTGCCGGAACCGATGGACAATTGTTCAGTC
PDFZ1092	TTCCGGCAATCATTCGTGCGTATTTAGTATC
PDFZ1097	GATGGCCGAAACTGCGTATTTCGATCAAGG
PDFZ1098	TTTCGGCCATCCAAAGGACTGGAACAACGAC
PDFZ1069	CAACGCCAACACCGGACTCACGTGCATCATC
PDFZ1070	TGTTGGCGTTGGTTACATAGTAATGCGAAGC
PDFZ1071	GAAGGCCACCACCGAGAAGTTCACGGTCACATTC
PDFZ1072	TGGTGGCCTTCTCGTTGAAGACCAAATTGAACTG
PDFZ1073	ATTCGCCGAGACAGTCAGTGTCGAAGGAGATTG
PDFZ1074	TCTCGGCGAATGTGACCGTGAACTTCTCGGTG

Data were considered statistically different at $P < 0.05$. $P < 0.05$ is indicated with single asterisks and $P < 0.0001$ with double asterisks (0.001 in a two-way ANOVA analysis).

Plasmid construction

$P_{scav\text{-}3}$SCAV-3::GFP reporter was created by a PCR fusion-based method (Hobert, 2002). In the first round of PCR, *scav-3* genomic DNA including the 2.7-kb promoter region was amplified using primers PWZ853 and PWZ855 and N2 genomic DNA as the template. GFP and the 3′UTR of *unc-54* were amplified from pPD49.26-GFP using PHWD478/PWZ512. The two PCR products were fused in the second round of PCR using PWZ854/PPFG199. The worm sfGFP (super-fold GFP) reporter was constructed by amplifying the sfGFP fragment from cc-HS4C3-sfGFP (H.E. Buelow, Albert Einstein College of Medicine, New York, NY) with primers PDFZ623/PDFZ624 and inserting it into pPD49.26 through the KpnI–EcoRV sites. $P_{scav\text{-}3}$SCAV-3::sfGFP was generated by first ligating the *scav-3* genomic DNA amplified with primers PWZ862 and PDFZ721 into pPD49.26-sfGFP through the NheI–MluI sites, followed by insertion of the *scav-3* promoter amplified by primers PWZ895 and PWZ896 at the HindIII–PstI sites. To generate $P_{scav\text{-}3}$SCAV-3(AAA)::sfGFP, the AAA mutation of SCAV-3 was introduced into $P_{scav\text{-}3}$SCAV-3::sfGFP by site-directed mutagenesis using primers PYL379 and PYL380. To express RAB-10 and RAB-11 in hypodermis, RAB-10 and RAB-11.1 fragments were digested from $P_{vha\text{-}6}$GFP::RAB-10 and $P_{vha\text{-}6}$GFP::RAB-11.1 and cloned into pPD49.26-$P_{hyp\text{-}7}$GFP1 through the KpnI site. $P_{hyp\text{-}7}$MANS::GFP was constructed by amplifying the MANS cDNA from a *C. elegans* cDNA library (Invitrogen) using primers PYTX95 and PYTX96 and ligating the product into pPD49.26-$P_{hyp\text{-}7}$GFP3 through the NheI–KpnI sites. To construct $P_{hyp\text{-}7}$GFP::TRAM, TRAM cDNA was amplified from the *C. elegans* cDNA library (Invitrogen) with primers PYJ45 and PBL727 and cloned into pPD49.26-$P_{hyp\text{-}7}$GFP1 through the KpnI site. To generate $P_{hyp\text{-}7}$sfGFP::Galectin3 (Gal3), Gal3 was amplified from ptf-Galectin3 (T. Yoshimori, Osaka University, Osaka, Japan) with primers PDFZ627/PDFZ628 and ligated into pPD49.26-$P_{hyp\text{-}7}$sfGFP1 through the EcoRV–SacI sites. The *hyp-7* promoter ($P_{hyp\text{-}7}$) was then replaced by $P_{vha\text{-}6}$, $P_{myo\text{-}3}$, or P_{hsp} through the BamHI site to generate sfGFP::Gal3 reporters specifically expressed in the intestine cells ($P_{vha\text{-}6}$), body wall muscle ($P_{myo\text{-}3}$), or pharynx (P_{hsp}). To construct $P_{hyp\text{-}7}$sfGFP::Galectin9 (Gal9), Gal9 was amplified from pENTR221-Galectin9 (Invitrogen) with primers PDFZ898/PDFZ899 and cloned into pPD49.26-$P_{hyp\text{-}7}$sfGFP1 through the EcoRV site. To generate $P_{hyp\text{-}7}$LMP-1::CeBFP and $P_{hyp\text{-}7}$LMP-2::CeBFP, LMP-1 and LMP-2 were amplified with primers PSZ46/PSZ47 and PXCW192/PXCW193, respectively, and ligated into pPD49.26-$P_{hyp\text{-}7}$ CeBFP3 through the KpnI site. $P_{hyp\text{-}7}$CTNS-1::CeBFP and $P_{hyp\text{-}7}$ LAAT-1::CeBFP were constructed by amplifying CTNS-1 and LAAT-1 fragments using primers PPFG227/PPFG228 and PBL516/PBL515, respectively, and cloning them into pPD49.26-$P_{hyp\text{-}7}$-CeBFP3 through the KpnI site. To construct $P_{Y105E8B.9}$Y105E8B.9::mCherry, the promoter region of *y105e8b.9* was amplified by primers PJCL257/PJCL258 and cloned to pPD49.26-cherry via the SphI–XmaI sites. The full-length genomic DNA of *y105e8b.9* amplified by PJCL249/PJCL439 was then inserted at the KpnI site. To generate P_{hsp}NUC-1::sfGFP::mmCherry, mmCherry was cloned into pPD49.26-sfGFP via the EcoRV–SacI sites, followed by insertion of NUC-1 at the XmaI–KpnI sites and P_{hsp} at the BamHI site. To generate $P_{lmp\text{-}1}$LMP-1::sfGFP and $P_{lmp\text{-}2}$LMP-2::sfGFP, LMP-1 or LMP-2 fragments were cloned into pPD49.26-sfGFP3 through the KpnI site, followed by insertion of the promoter of *lmp-1* or *lmp-2* amplified using primers PBL520/PBL521 or PDFZ989/PDFZ990 at the PstI–XmaI sites. To generate $P_{scav\text{-}3}$SCAV-3(G279R)::sfGFP and $P_{scav\text{-}3}$SCAV-3(S382F)::sfGFP, site-directed mutagenesis was performed to introduce mutations into $P_{scav\text{-}3}$SCAV-3::sfGFP by primers PYL365/PYL366 and PYL367/PYL368, respectively. $P_{scav\text{-}3}$SCAV-3::CeBFP was constructed by first ligating the *scav-3* genomic DNA amplified with primers PWZ862 and PDFZ721 into pPD49.26 through the NheI–MluI sites, followed by insertion of CeBFP amplified by primers PYL404 and PWZ985 at the MluI–SacI sites. The *scav-3* promoter was then amplified by primers PYL405 and PDFZ999 and inserted at the PstI–XmaI sites. Mutations in the glycosylation sites of SCAV-3 were introduced into $P_{scav\text{-}3}$SCAV-3::sfGFP and $P_{scav\text{-}3}$SCAV-3::CeBFP by site-directed mutagenesis using primers PDFZ1079/PDFZ1080 (N53A), PDFZ1081/PDFZ1082(N80A), PDFZ1083/PDFZ1084(N118A), PDFZ1087/PDFZ1088(N233A), PDFZ1091/PDFZ1092(N278A), and PDFZ1097/PDFZ1098 (N456A). Mutations in the glycosylation sites of LMP-1 were introduced into $P_{hyp\text{-}7}$LMP-1::CeBFP by site-directed mutagenesis using primers PDFZ1069/PDFZ1070 (N27A), PDFZ1071/PDFZ1072(N50A), and PDFZ1073/PDFZ1074 (N60A). See Table 1 for a list of primers used for plasmid construction.

Online supplemental material

Fig. S1 shows that loss of *scav-3* affects lysosome morphology and dynamics. Fig. S2 shows the molecular cloning of *scav-3*. Fig. S3 shows that *scav-3(qx193)* mutants accumulate damaged lysosomes. Fig. S4 shows that glycosylation is important for the stability and lysosomal targeting of SCAV-3. Fig. S5 shows that overexpression of LMP-1 or reduced activity of *daf-2* does not reverse the abnormal lysosome morphology and dynamics in *scav-3(qx193)*. Videos 1–4 show appearance of damaged lysosomes in *scav-3* mutants expressing GFP::Gal3 and NUC-1::mCherry (Video 1), GBA-3::mCherry (Video 2), CPL-1::mCherry (Video 3), and CPR-6::mCherry (Video 4).

Acknowledgments

We thank Drs. K. Ravichandran, M.O. Hengartner, B. Grant, S. Mitani, G. Hermann, T. Yoshimori, and H. E. Buelow for strains and plasmids and Dr. Isabel Hanson for editing services.

This work was supported by the Chinese Ministry of Science and Technology (2016YFA0500203), the National Basic Research Program of China (2013CB910100 and 2014CB849702), the National Natural Science Foundation of China (31325015), and an International Early Career Scientist grant from the Howard Hughes Medical Institute to X. Wang. Some strains were provided by the Caenorhabditis Genetics Center, which is funded by the National Institutes of Health Office of Research Infrastructure Programs (P40OD010440).

The authors declare no competing financial interests.

Submitted: 28 February 2016
Accepted: 13 September 2016

References

Anisimov, V.N., and A. Bartke. 2013. The key role of growth hormone-insulin-IGF-1 signaling in aging and cancer. *Crit. Rev. Oncol. Hematol.* 87:201–223. http://dx.doi.org/10.1016/j.critrevonc.2013.01.005

Appelqvist, H., P. Wäster, K. Kågedal, and K. Öllinger. 2013. The lysosome: From waste bag to potential therapeutic target. *J. Mol. Cell Biol.* 5:214–226. http://dx.doi.org/10.1093/jmcb/mjt022

Berkovic, S.F., L.M. Dibbens, A. Oshlack, J.D. Silver, M. Katerelos, D.F. Vears, R. Lüllmann-Rauch, J. Blanz, K.W. Zhang, J. Stankovich, et al. 2008. Array-based gene discovery with three unrelated subjects shows SCARB2/LIMP-2 deficiency causes myoclonus epilepsy and glomerulosclerosis. *Am. J. Hum. Genet.* 82:673–684. http://dx.doi.org/10.1016/j.ajhg.2007.12.019

Blanz, J., J. Groth, C. Zachos, C. Wehling, P. Saftig, and M. Schwake. 2010. Disease-causing mutations within the lysosomal integral membrane

protein type 2 (LIMP-2) reveal the nature of binding to its ligand beta-glucocerebrosidase. *Hum. Mol. Genet.* 19:563–572. http://dx.doi.org/10.1093/hmg/ddp523

Brenner, S. 1974. The genetics of *Caenorhabditis elegans*. *Genetics.* 77:71–94.

Calfon, M., H. Zeng, F. Urano, J.H. Till, S.R. Hubbard, H.P. Harding, S.G. Clark, and D. Ron. 2002. IRE1 couples endoplasmic reticulum load to secretory capacity by processing the XBP-1 mRNA. *Nature.* 415:92–96. http://dx.doi.org/10.1038/415092a

Cuervo, A.M., and J.F. Dice. 2000. When lysosomes get old. *Exp. Gerontol.* 35:119–131. http://dx.doi.org/10.1016/S0531-5565(00)00075-9

de Duve, C. 1983. Lysosomes revisited. *Eur. J. Biochem.* 137:391–397. http://dx.doi.org/10.1111/j.1432-1033.1983.tb07841.x

de Voer, G., D. Peters, and P.E. Taschner. 2008. *Caenorhabditis elegans* as a model for lysosomal storage disorders. *Biochim. Biophys. Acta.* 1782:433–446. http://dx.doi.org/10.1016/j.bbadis.2008.04.003

Eskelinen, E.L. 2006. Roles of LAMP-1 and LAMP-2 in lysosome biogenesis and autophagy. *Mol. Aspects Med.* 27:495–502. http://dx.doi.org/10.1016/j.mam.2006.08.005

Eskelinen, E.L., C.K. Schmidt, S. Neu, M. Willenborg, G. Fuertes, N. Salvador, Y. Tanaka, R. Lüllmann-Rauch, D. Hartmann, J. Heeren, et al. 2004. Disturbed cholesterol traffic but normal proteolytic function in LAMP-1/LAMP-2 double-deficient fibroblasts. *Mol. Biol. Cell.* 15:3132–3145. http://dx.doi.org/10.1091/mbc.E04-02-0103

Evans, T.C., editor. 2005. Transformation and microinjection. *In* Wormbook. The Online Review of *C. elegans* Biology. doi:http://dx.doi.org/10.1895/wormbook.1.7.1, http://www.wormbook.org/.

Fehrenbacher, N., L. Bastholm, T. Kirkegaard-Sørensen, B. Rafn, T. Bøttzauw, C. Nielsen, E. Weber, S. Shirasawa, T. Kallunki, and M. Jäättelä. 2008. Sensitization to the lysosomal cell death pathway by oncogene-induced down-regulation of lysosome-associated membrane proteins 1 and 2. *Cancer Res.* 68:6623–6633. http://dx.doi.org/10.1158/0008-5472.CAN-08-0463

French, A.P., S. Mills, R. Swarup, M.J. Bennett, and T.P. Pridmore. 2008. Colocalization of fluorescent markers in confocal microscope images of plant cells. *Nat. Protoc.* 3:619–628. http://dx.doi.org/10.1038/nprot.2008.31

Fukuda, M. 1991. Lysosomal membrane glycoproteins. Structure, biosynthesis, and intracellular trafficking. *J. Biol. Chem.* 266:21327–21330.

Gamp, A.C., Y. Tanaka, R. Lüllmann-Rauch, D. Wittke, R. D'Hooge, P.P. De Deyn, T. Moser, H. Maier, D. Hartmann, K. Reiss, et al. 2003. LIMP-2/LGP85 deficiency causes ureteric pelvic junction obstruction, deafness and peripheral neuropathy in mice. *Hum. Mol. Genet.* 12:631–646. http://dx.doi.org/10.1093/hmg/ddg062

Gonzalez, A., M. Valeiras, E. Sidransky, and N. Tayebi. 2014. Lysosomal integral membrane protein-2: A new player in lysosome-related pathology. *Mol. Genet. Metab.* 111:84–91. http://dx.doi.org/10.1016/j.ymgme.2013.12.005

Groth-Pedersen, L., and M. Jäättelä. 2013. Combating apoptosis and multidrug resistant cancers by targeting lysosomes. *Cancer Lett.* 332:265–274. http://dx.doi.org/10.1016/j.canlet.2010.05.021

Guo, P., T. Hu, J. Zhang, S. Jiang, and X. Wang. 2010. Sequential action of *Caenorhabditis elegans* Rab GTPases regulates phagolysosome formation during apoptotic cell degradation. *Proc. Natl. Acad. Sci. USA.* 107:18016–18021. http://dx.doi.org/10.1073/pnas.1008946107

Hansen, M., A.L. Hsu, A. Dillin, and C. Kenyon. 2005. New genes tied to endocrine, metabolic, and dietary regulation of lifespan from a *Caenorhabditis elegans* genomic RNAi screen. *PLoS Genet.* 1:119–128. http://dx.doi.org/10.1371/journal.pgen.0010017

Hobert, O. 2002. PCR fusion-based approach to create reporter gene constructs for expression analysis in transgenic *C. elegans*. *Biotechniques.* 32:728–730.

Hochschild, R. 1971. Lysosomes, membranes and aging. *Exp. Gerontol.* 6:153–166. http://dx.doi.org/10.1016/S0531-5565(71)80014-1

Hung, Y.H., L.M. Chen, J.Y. Yang, and W.Y. Yang. 2013. Spatiotemporally controlled induction of autophagy-mediated lysosome turnover. *Nat. Commun.* 4:2111. http://dx.doi.org/10.1038/ncomms3111

Kallunki, T., O.D. Olsen, and M. Jäättelä. 2013. Cancer-associated lysosomal changes: Friends or foes? *Oncogene.* 32:1995–2004. http://dx.doi.org/10.1038/onc.2012.292

Kamath, R.S., and J. Ahringer. 2003. Genome-wide RNAi screening in *Caenorhabditis elegans*. *Methods.* 30:313–321. http://dx.doi.org/10.1016/S1046-2023(03)00050-1

Kostich, M., A. Fire, and D.M. Fambrough. 2000. Identification and molecular-genetic characterization of a LAMP/CD68-like protein from *Caenorhabditis elegans*. *J. Cell Sci.* 113:2595–2606.

Kreuzaler, P., and C.J. Watson. 2012. Killing a cancer: What are the alternatives? *Nat. Rev. Cancer.* 12:411–424. http://dx.doi.org/10.1038/nrc3264

Kundra, R., and S. Kornfeld. 1999. Asparagine-linked oligosaccharides protect Lamp-1 and Lamp-2 from intracellular proteolysis. *J. Biol. Chem.* 274:31039–31046. http://dx.doi.org/10.1074/jbc.274.43.31039

Kuronita, T., E.L. Eskelinen, H. Fujita, P. Saftig, M. Himeno, and Y. Tanaka. 2002. A role for the lysosomal membrane protein LGP85 in the biogenesis and maintenance of endosomal and lysosomal morphology. *J. Cell Sci.* 115:4117–4131. http://dx.doi.org/10.1242/jcs.00075

Lewis, V., S.A. Green, M. Marsh, P. Vihko, A. Helenius, and I. Mellman. 1985. Glycoproteins of the lysosomal membrane. *J. Cell Biol.* 100:1839–1847. http://dx.doi.org/10.1083/jcb.100.6.1839

Liu, B., H. Du, R. Rutkowski, A. Gartner, and X. Wang. 2012. LAAT-1 is the lysosomal lysine/arginine transporter that maintains amino acid homeostasis. *Science.* 337:351–354. http://dx.doi.org/10.1126/science.1220281

Maejima, I., A. Takahashi, H. Omori, T. Kimura, Y. Takabatake, T. Saitoh, A. Yamamoto, M. Hamasaki, T. Noda, Y. Isaka, and T. Yoshimori. 2013. Autophagy sequesters damaged lysosomes to control lysosomal biogenesis and kidney injury. *EMBO J.* 32:2336–2347. http://dx.doi.org/10.1038/emboj.2013.171

Murphy, C.T., and P.J. Hu. 2013. Insulin/insulin-like growth factor signaling in *C. elegans*. *WormBook.* 26:1–43. http://dx.doi.org/10.1895/wormbook.1.164.1

Neculai, D., M. Schwake, M. Ravichandran, F. Zunke, R.F. Collins, J. Peters, M. Neculai, J. Plumb, P. Loppnau, J.C. Pizarro, et al. 2013. Structure of LIMP-2 provides functional insights with implications for SR-BI and CD36. *Nature.* 504:172–176. http://dx.doi.org/10.1038/nature12684

Orenstein, S.J., and A.M. Cuervo. 2010. Chaperone-mediated autophagy: Molecular mechanisms and physiological relevance. *Semin. Cell Dev. Biol.* 21:719–726. http://dx.doi.org/10.1016/j.semcdb.2010.02.005

Paz, I., M. Sachse, N. Dupont, J. Mounier, C. Cederfur, J. Enninga, H. Leffler, F. Poirier, M.C. Prevost, F. Lafont, and P. Sansonetti. 2010. Galectin-3, a marker for vacuole lysis by invasive pathogens. *Cell. Microbiol.* 12:530–544. http://dx.doi.org/10.1111/j.1462-5822.2009.01415.x

Reczek, D., M. Schwake, J. Schröder, H. Hughes, J. Blanz, X. Jin, W. Brondyk, S. Van Patten, T. Edmunds, and P. Saftig. 2007. LIMP-2 is a receptor for lysosomal mannose-6-phosphate-independent targeting of beta-glucocerebrosidase. *Cell.* 131:770–783. http://dx.doi.org/10.1016/j.cell.2007.10.018

Repnik, U., M. Hafner Česen, and B. Turk. 2014. Lysosomal membrane permeabilization in cell death: Concepts and challenges. *Mitochondrion.* 19(Pt A):49–57. http://dx.doi.org/10.1016/j.mito.2014.06.006

Saftig, P., B. Schröder, and J. Blanz. 2010. Lysosomal membrane proteins: Life between acid and neutral conditions. *Biochem. Soc. Trans.* 38:1420–1423. http://dx.doi.org/10.1042/BST0381420

Settembre, C., A. Fraldi, D.L. Medina, and A. Ballabio. 2013. Signals from the lysosome: A control centre for cellular clearance and energy metabolism. *Nat. Rev. Mol. Cell Biol.* 14:283–296. http://dx.doi.org/10.1038/nrm3565

Terman, A., and U.T. Brunk. 1998. Lipofuscin: Mechanisms of formation and increase with age. *APMIS.* 106:265–276. http://dx.doi.org/10.1111/j.1699-0463.1998.tb01346.x

Thurston, T.L., M.P. Wandel, N. von Muhlinen, A. Foeglein, and F. Randow. 2012. Galectin 8 targets damaged vesicles for autophagy to defend cells against bacterial invasion. *Nature.* 482:414–418. http://dx.doi.org/10.1038/nature10744

Tian, Y., Z. Li, W. Hu, H. Ren, E. Tian, Y. Zhao, Q. Lu, X. Huang, P. Yang, X. Li, et al. 2010. *C. elegans* screen identifies autophagy genes specific to multicellular organisms. *Cell.* 141:1042–1055. http://dx.doi.org/10.1016/j.cell.2010.04.034

Treusch, S., S. Knuth, S.A. Slaugenhaupt, E. Goldin, B.D. Grant, and H. Fares. 2004. *Caenorhabditis elegans* functional orthologue of human protein h-mucolipin-1 is required for lysosome biogenesis. *Proc. Natl. Acad. Sci. USA.* 101:4483–4488. http://dx.doi.org/10.1073/pnas.0400709101

Vega, M.A., B. Seguí-Real, J.A. García, C. Calés, F. Rodríguez, J. Vanderkerckhove, and I.V. Sandoval. 1991. Cloning, sequencing, and expression of a cDNA encoding rat LIMP II, a novel 74-kDa lysosomal membrane protein related to the surface adhesion protein CD36. *J. Biol. Chem.* 266:16818–16824.

Zachos, C., J. Blanz, P. Saftig, and M. Schwake. 2012. A critical histidine residue within LIMP-2 mediates pH sensitive binding to its ligand β-glucocerebrosidase. *Traffic.* 13:1113–1123. http://dx.doi.org/10.1111/j.1600-0854.2012.01372.x